UNIVERSIDADE DE LISBOA
FACULDADE DE CIÊNCIAS
DEPARTAMENTO DE FÍSICA

EEG Spectral Analysis as a Predictor of Popularity

Rafael Alexandre Santos Marques

Mestrado em Engenharia Biomédica e Biofísica

Dissertação orientada por:
Dr. Diego Andrés Blanco-Mora
Prof. Alexandre Andrade

2023

Abstract

The present research is part of the eMOTIONAL Cities project, which investigates how urban environments affect cognitive and emotional processes. The study involved electroencephalography (EEG) to analyse whether brain responses can predict the popularity of urban spaces shown to the participants and whether there are differences between images taken by tourists and residents.

EEG is a non-invasive technique widely used in neuroimaging due to its high temporal resolution. To improve spatial resolution, high-density EEG uses many electrodes (usually 128 or 256).

One way to assess brain activity with EEG is through Event-Related Potentials (ERPs), which are brain responses to events such as visual and auditory stimuli. A baseline period is used to normalize the time-frequency version of ERPs known as Event Related Spectral Perturbation (ERSP). An interactive 3D graph containing time, frequency, and power serves as the ERSP representation. This graph is produced by convolution with complex Morlet waves, which guarantees good temporal and frequency resolution.

The EEG data, obtained from the frontal cortex, was pre-processed to remove artefacts and improve quality. Time-frequency analysis revealed three significant time-frequency regions, in which were named as: alpha, alpha-beta and beta spots. The alpha spot can be related to visual processing, while alpha-beta and beta spots are linked to decision-making. Tourist group showed higher ERSP values in the alpha region and a correlation with popularity ($r = 0.24, p < 0.05$) was found. Regarding alpha-beta spot, residents had slightly higher values, but no significant correlation with popularity ($r = 0.07, p > 0.05$) was found. In the beta region, residents had more scattered data, and tourists had higher ERPs, with an insignificant correlation ($r = 0.05,\ p > 0.05$) between ERS/ERD and popularity. In summary, alpha activity from the frontal cortex provides valuable insights into predicting the popularity of the urban places shown, and there are no differences between residents and tourists.

Keywords: EEG signals, ERS/ERD, predictor, time-frequency, urban spaces.

Resumo

A eletroencefalografia (EEG) é uma técnica não invasiva que permite medir os campos elétricos gerados pela corrente elétrica cerebral. Esta é uma técnica bastante utilizada em neuroimagem devido à sua excelente resolução temporal. Para colmatar a fraca resolução espacial, foi desenvolvida EEG de alta densidade que consiste num número elevado de elétrodos no capacete de EEG (normalmente 128 ou 256). A eletroencefalografia de alta densidade é muitas vezes associada à ressonância magnética, uma vez que a conjunção de ambas as técnicas garante uma elevada resolução temporal e espacial, para além de permitir uma melhor reconstrução das fontes de atividade cerebral.

Uma das diversas formas de avaliar a atividade cerebral com EEG é recorrendo aos potenciais relacionados a eventos (ERPs) que são criados por certos eventos, como por exemplo estímulos visuais e auditivos. Estes ERPs podem ser quantificados usando o método de dessincronização/sincronização. A dessincronização (ERD, do inglês 'Event-Related Desynchronization') representa uma diminuição da amplitude do EEG após o estímulo, enquanto que a sincronização (ERS, do inglês 'Event-Related Synchronization') simboliza um aumento da amplitude do EEG após o estímulo.

A presente dissertação encontra-se associada à experiência *Brain as Predictor* (BAP) que pertence ao projeto *eMOTIONAL Cities*. O objetivo maior deste projeto é obter evidências de como os espaços urbanos moldam os processos cognitivos e emocionais do ser humano. A experiência BAP recorreu a EEG e fMRI (functional Magnetic Resonance Imaging), em simultâneo, para estudar a atividade cerebral e avaliar o potencial dessa mesma atividade como fator de previsão dos espaços urbanos no ser humano. Já em relação ao objetivo concreto da presente dissertação, este prende-se em dois pontos. Primeiramente, pretende-se verificar se a análise espetral dos sinais de EEG pode servir como fator de previsão da popularidade dos espaços urbanos. Para além disto, pretende-se verificar se existe diferença significativa na análise espetral dos sinais de EEG entre as imagens tiradas por turistas e as fotografias tiradas por residentes, recorrendo para tal a um boxplot de violino.

A experiência *Brain as Predictor* tem como objetivo averiguar se a atividade cerebral pode ser utilizada para prever a forma como os ambientes urbanos afetam as pessoas, nomeadamente a atividade do córtex frontal, visto que é uma zona proeminente no que toca a tarefas de memória de curto prazo e atenção. Para este estudo recorreu-se estímulos visuais que consistiam em imagens de diferentes ambientes urbanos de Lisboa (uns mais turísticos e outros mais urbanos). Os sujeitos saudáveis participaram na experiência, na qual classificaram cada imagem utilizando um joystick numa escala de 1 a 4. A experiência seguiu um paradigma específico, incluindo intervalos de ecrã em branco, apresentação de cruzes pretas, apresentação de imagens e classificação por estrelas, cada uma com intervalos de tempo definidos. Os participantes passaram por duas sessões com 80 imagens cada, perfazendo a duração total de cada tarefa 640 segundos. O processo completo de aquisição de dados durou 1280 segundos. Para esta experiência foram recrutados 25 participantes saudáveis com idades compreendidas entre os 18 e 35 anos ($média = 23.1$ e $std = 3.24$).

De modo a analisar os dados provenientes da eletroencefalografia, foi necessário fazer um pré-processamento para limpar o sinal. Os sinais de EEG são frequentemente ruidosos, pelo que a limpeza é um passo crucial para uma correta análise. O processo compreendeu várias etapas, como a remoção de artefactos, a resolução de um efeito de corte residual nos dados, a remoção de canais desnecessários, a redução da amostragem dos dados para eficiência computacional, a aplicação de um filtro passa-banda para limitar a informação de frequência, a limpeza agressiva para remover canais e partes de dados com ruído, a interpolação para colmatar a ausência de canais ruidosos e, finalmente, a re-referenciação dos dados EEG utilizando a referenciação média. A Análise de Componentes Independentes (ICA) foi

também efetuada para classificar os componentes em diferentes categorias, sendo listados em: cérebro, músculo, olho, coração, ruído de linha, ruído de canal e outros, com valores de limiar específicos para rejeição.

Para analisar estes potenciais, é muito recorrente utilizar o domínio tempo-frequência dos ritmos do EEG. Esta análise consiste num gráfico 3D com o tempo e a frequência nos eixos *xx* e *yy*, respetivamente, e uma outra variável no eixo *zz*, como por exemplo a amplitude. Para obter o gráfico no domínio tempo-frequência, foi utilizado o método da convolução com *wavelets*, com o sinal do EEG e em diversas frequências pertencentes às ondas cerebrais. Este método é uma alternativa ao espetrograma convencional e garante uma ótima resolução temporal e em frequência. Para fazer esta convolução, as *wavelets* de Morlet complexas foram sobrepostas ao EEG pré-processado. Após a convolução, os valores de potência resultantes foram extraídos de frequências de 8 a 30 Hz e de -1 a 4 segundos em relação ao início do estímulo. Foi escolhida uma onda de 10 ciclos para equilibrar a resolução temporal e de frequência. A análise principal teve como objetivo comparar as respostas do EEG a imagens tiradas por residentes e turistas. Os conjuntos de dados EEG foram carregados, segmentados, e analisados dentro das bandas de frequência alfa e beta, aplicando uma correção da linha de base. Os ensaios com tempos de reação inferiores a 1 segundo foram excluídos. A qualidade dos dados foi ainda melhorada através da remoção de épocas com potência excessiva em bandas de frequência específicas. As representações tempo-frequência de todos os ensaios foram traçadas e foram aplicadas máscaras estatísticas para identificar pontos significativos com base em testes t. Foi efetuada uma comparação entre imagens de residentes e de turistas utilizando boxplots e gráficos de violino. Além disso, o coeficiente de correlação de Spearman foi utilizado para explorar a relação entre as respostas EEG (ERS/ERD) e a popularidade da imagem para os pontos significativos.

Após a análise tempo-frequência, foi aplicada uma máscara estatística que identificou três regiões significativas que foram nomeadas com base na gama de frequências pertencentes: região alfa, região alfa-beta e região beta. A região na banda alfa está associada ao processamento de estímulos visuais, marcadas por ERD, indicando ativação cortical durante a visualização de imagens. As regiões alfa-beta e beta estão relacionadas com a tomada de decisões, marcadas por ERS, indicando uma redução do processamento de informações no córtex frontal. Na zona alfa, a população dos turistas apresenta valores de ERS/ERD mais elevados e com menor variabilidade do que o grupo dos residentes. Apesar disto, ambos os grupos parecem ser estatisticamente semelhantes ($p = 0.87$). Foi evidenciada uma correlação entre popularidade e ERS/ERD ($r = 0.24, p < 0.05$). Para a zona alfa-beta, a população dos residentes apresenta valores de ERS/ERD ligeiramente superiores, porém ambos os grupos apresentam uma variabilidade semelhante. O t-test aplicado evidencia a identidade estatística entre ambas as populações ($p = 0.30$). A popularidade não se correlacionou significativamente com a ERS/ERD ($r = 0.07, p > 0.05$). Na zona da banda beta, a população dos residentes tinha dados mais dispersos e o grupo dos turistas tinha valores ERS/ERD mais elevados. A análise estatística sugere que as populações não são estatisticamente diferentes ($p = 0.54$). A relação entre popularidade e ERS/ERD foi insignificante ($r = 0.05,\ p > 0.05$). De modo geral, os valores de ERS/ERD diferiram em ambas as populações em várias regiões das bandas de frequência, mas o seu poder preditivo para a popularidade da imagem foi evidente apenas na zona da banda alfa. Em resumo, a atividade do ritmo alfa no córtex frontal fornece informações valiosas para prever a popularidade dos locais urbanos apresentados nas imagens.

Palavras-Chave: ERS/ERD, espaços urbanos, preditor, sinais EEG, tempo-frequência.

Acknowledgment

First, I would like to thank to my family for supporting me during all this process, namely, my mother (Helena Marques), father (Rui Marques), brothers (Miguel Marques and Daniel Marques), aunts (Teresa Santos and Paula Palhão), uncles (Filipe Santos and Alexandre Santos), cousins (Jessica Oliveira and Frederica Oliveira) and sister-in-law (Sara Paulo).

I also would like to acknowledge my friends. First, the ones that were around me since day one of university: Beatriz Rodrigues, Daniel Simão, Duarte Cunha, Guilherme Silva, Hayanna Valle and Maria Gonçalves. Then, I want to thank to my friends that grew up with me: Beatriz Tomás, Carolina Marques, Daniel Marques, Francisco Carvalho, Irina Jorge, Ivo Pina and Sofia Martinho. Finally, I want to thank to some other friends that had a big impact in my life during the past 5 years, in different ways: André Coelho, Cláudia Reis, Daniel Silva, David Pereira, Francisco Carneiro, Henrique Lopes, Inês Lopes, Inês Veloso, Joana Carvoeiro, Laura Martins, Leonor Carvalho, Manuel Dias, Mariana Morais, Mariana Oliveira, Miguel Leocádio, Rafael Santos and Rui Batista. All these friends were an essential part of this journey and made me feel better when I was not in my happy days.

Then, I would like to thank Dr. Diego Andrés-Blanco Mora for all the support during these months, namely all the knowledge he gave me in the EEG measurements and signal processing. Also, I would like to acknowledge Prof. Alexandre Andrade for helping me finding a path to my master thesis and for always being able to help me during this journey.

Last but not least, I would like to thank me for not giving up in the moments that I was feeling down and for finishing this master thesis.

Table of Contents

List of Figures

List of Tables

List of Equations

List of Abbreviations

- **ACad** – Rostral-Ventral Affective Division
- **ACC** – Anterior Cingulate Cortex
- **ACcd** – Dorsal Cognitive Division
- **ART** – Attention-Restoration Theory
- **BAP** – Brain as Predictor
- **BA17** – Brodmann Area 17
- **BA18** – Brodmann Area 18
- **BA19** – Brodmann Area 19
- **BA25** – Brodmann Area 25
- **BCG** – Ballistocardiograph
- **BIS/BAS** – Behavioural Inhibition System/Behavioural Activation System
- **BOLD** – Blood-Oxygen-Level-Dependent
- **BNST** – Bed Nucleus of the Stria Terminalis
- **cm** – centimetres
- **COVID-19** – Coronavirus Disease 2019
- **CT** – Computed Tomography
- **CWT** – Continuous Wavelet Transform
- **DASS-21** – Depression Anxiety and Stress Scale
- **DFT** – Discrete Fourier Transform
- **ECG** – Electrocardiography
- **EDA** – Electrodermal Activity
- **EEG** – Electroencephalography
- **EGI** – Electrical Geodesics, Inc
- **ERD** – Event-Related Desynchronization
- **ERP** – Event-Related Potential
- **ERS** – Event-Related Synchronization
- **ERSP** – Event Related Spectral Perturbation
- **FFT** – Fast Fourier Transform
- **FID** – Free Induction Decay
- **FMUL** – Faculdade de Medicina da Universidade de Lisboa
- **fMRI** – Functional Magnetic Resonance Imaging
- **GES** – GStreamer Editing Services
- **GPi** – Globus Pallidus Internus
- **HD-EEG** – High Density Electroencephalography
- **Hz** – Hertz
- **ICA** – Independent Component Analysis
- **ID** – Identity
- **IFG** – Inferior Frontal Gyrus
- **IGOT** – Instituto de Geografia e Ordenamento do Território
- **kHz** – Kilohertz
- **LP** – Left Preauricular
- **L** – Litres

- **MEMS** – Microelectromechanical Systems
- **ml** – millilitres
- **mm** – millimetres
- **mPFC** – Medial Prefrontal Cortex
- **ms** – Milliseconds
- **MRI** – Magnetic Resonance Imaging
- **mV** – Millivolts
- **NAc** – *Nucleus Accumbens*
- **NREM** – Non-Rapid Eye Movement
- **PANAS** – Positive and Negative Affect Schedule
- **PCun** – *Precuneus*
- **PLV** – Phase-Locking Value
- **PM** – Post Meridiem
- **PSD** – Power Spectral Density
- **PSP** – Postsynaptic Potentials
- **REM** – Rapid Eye Movement
- **RF** – Radiofrequency
- **RP** – Right Preauricular
- **SNc** – *Substantia Nigra pars Compacta*
- **SNR** – Signal-to-Noise Ratio
- **SNr** – *Substantia Nigra pars Reticulata*
- **SPC** – Superior Parietal Cortex
- **Std** – Standard Deviation
- **STFT** – Short-Time Fourier Transform
- **STG** – Superior Temporal Gyrus
- **T** – Tesla
- **TE** – Echo Time
- **TR** – Repetition Time
- **VTA** – Ventral Tegmental Area
- **V1** – Primary Visual Cortex
- **V2** – Secondary Visual Cortex
- **WPT** – Wavelet Packet Transform (WPT)
- **WT** – Wavelet Transform
- **WVD** – Wigner-Ville Distribution (WVD)
- **Ωm** – Ohm

1. Contextualization

The present dissertation is part of big international project called *eMOTIONAL Cities* (the logo is represented in **Figure 1.1**), which has a lot of partners. The main goal of this project is to investigate how urban environments affect people's cognitive and emotional processes.

To develop this thesis, I worked on an experiment called *Brain as Predictor*, inserted on *eMOTIONAL Cities* project. The main aim of this study was see if the brain activity can be used as predictor for evaluating the impact of urban environments on human beings. For that, EEG-fMRI was used, which is a very powerful tool for this type of cognitive studies since we have high spatial resolution form MRI and also high temporal resolution form EEG.

Although the *Brain as Predictor* study used EEG-fMRI, I only used the EEG signals do expand my master dissertation. I was particular interested on ERPs, meaning Event-Related Potentials. Basically, and ERP is brain activity caused by a certain type of events, for instance visual and auditory stimuli.

***Figure 1.1**: eMOTIONAL Cities logo.*

2. Background

In this chapter, some important concepts about electroencephalography, signal processing and neuroanatomy will be described.

2.1. Electroencephalography

2.1.1. History of Electroencephalography

The discovery of brain electric current was made by Richard Caton, an English physician, in 1875. Caton used non-polarizing electrodes in rabbits' and monkeys' brains (Collura, 1993; Teplan, 2002). However, humankind had to wait until 1924, when the German neurologist Hans Berger made the first acquisition of human brain activity (La Vaque, 1999; Teplan, 2002).

Berger was always interested in physics and, particularly, the physics behind the human mind. After finishing his medicine degree, Berger spent many years trying to measure the "mind energy" (La Vaque, 1999). In 1924, he had the idea to start a study with patients that were submitted to trepanation – surgical act in which the skull is opened, exposing the brain of the living be (Verano, 2016) – in order to measure the mind energy. In this way, in July 6th 1924 Berger was able to record 1 minute of almost microscopic vibrations placing electrodes on the skull of a 17-years-old patient who was submitted to trepanation – being this the first registration of human brain electrical activity ever made (La Vaque, 1999), to be later known as electroencephalography. On the following years, Berger tried to improve his technique utilizing electrodes with saline solution. Between 1929 and 1938, Hans Berger wrote 14 papers in which he explained his experiments and electroencephalography functioning (La Vaque, 1999).

2.1.2. Bioelectricity

In addition to offering priceless insights into the functioning of the human brain, Berger's groundbreaking work also paved the way for the study of bioelectricity. Therefore, it must be explored the world of neurons to comprehend the inner workings of the brain.

Stimuli received from sensory organs are transmitted along nerve fibres, and neurons (cells that take in sensory information from the outside world, provide motor orders to the muscles, and transform and relay electrical signals at each stage along the way) (Cooper et al., 2014; *What Is a Neuron? - Queensland Brain Institute - University of Queensland*, n.d.). However, for a nerve impulse to be transmitted, an action potential must occur. Action potentials (Moreira, 2015) consist in rapid changes in neuronal membrane potential.

Resting membrane potential is defined as the potential difference between the intracellular and extracellular spaces and it is typically -60 mV (Plonsey et al., 2007). When the cell membrane is stimulated and reaches the value above the excitatory limit (around -55 to -50 mV), the action potential is triggered. Action potentials can be divided into three phases (Plonsey et al., 2007), as shown in **Figure 2.1**

- **Depolarization** (light blue) – Due to the stimulus intensity above the threshold, the permeability of the cell membrane is changed, allowing a rapid influx of sodium ions into the intracellular space (passive transport), which raises the membrane potential to near +40 mV;
- **Repolarization** (light yellow) – When the action potential reaches its maximum during depolarization, there is an increase in the permeability to potassium ions, which causes their outflow into the extracellular space;
- **Hyperpolarization** (light red) – The result of all ionic exchange makes the intracellular space more negative than the resting potential. This causes a slight rise in the membrane potential to its resting value.

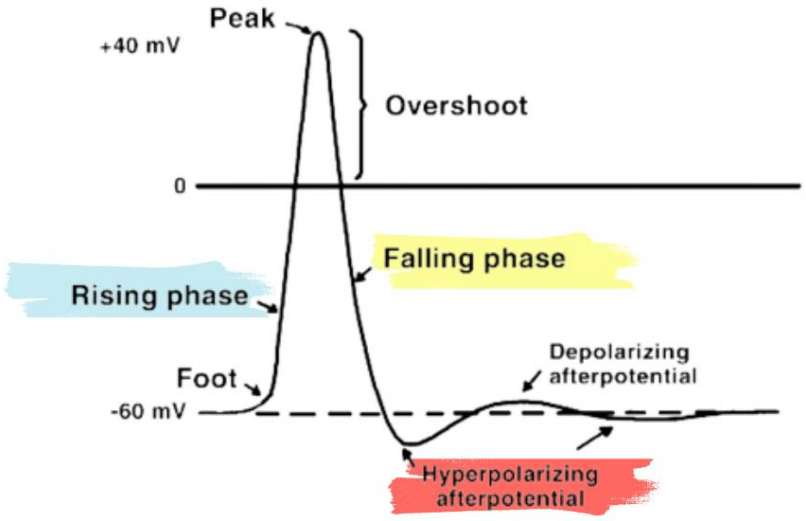

***Figure 2.1**: The three phases of the action potential: depolarization ('Rising phase'), repolarization ('Falling phase') and hyperpolarization ('Hyperpolarizing afterpotential'). Adapted from* (Plonsey et al., 2007).

The action potential is propagated from a cell to another through synapse, a specialized junction between the neuron and its target cell.

2.1.3. What is the EEG?

EEG is a non-invasive measurement of the electric fields generated by the brain's electric current. This requires placing electrodes along the scalp to record the potential differences created (Biasiucci et al., 2019; Teplan, 2002).

When neurons are activated due to the action potential, there will be a difference in the action potential at the level of these local neurons. However, it is important to note that only the activation of a large quantity of neurons can be measured with EEG (Teplan, 2002). In order to summarise this paragraph, the EEG will record the activity created by a large population of neurons (Biasiucci et al., 2019), as illustrated in **Figure 2.2**.

Although it seems a great neuroimaging method, the main signal source is from pyramidal neurons (Kirschstein & Köhling, 2009). This is a constraint because there are no pyramidal neurons in every single layer and brain regions.

It is important to keep in mind that the EEG does not measure action potentials, but rather the sum of excitatory and inhibitory postsynaptic potentials (PSP) (Cohen, 2014). PSP are known as a brief shift in the electric polarization of the membrane of a nerve cell. This is because the action potential occurs in a very brief period of time. Postsynaptic potentials, on the other hand, are the result of somewhat slower currents that follow the release of neurotransmitters at the axon's terminal boutons (Biasiucci et al., 2019).

Electroencephalography is one of the most used techniques in neuroimaging, since it presents an excellent temporal resolution – within milliseconds range (Gevins et al., 1999) – and can also acquire good spatial resolution when a high number of electrodes are used – typically 128 and 256. Furthermore, it is relatively cheap, easy to transport and totally safe (Di Flumeri et al., 2019; Rodrigues et al., 2021), compared to other neuroimaging tools, such as MRI (Magnetic Resonance Imaging) and CT (Computed Tomograhy).

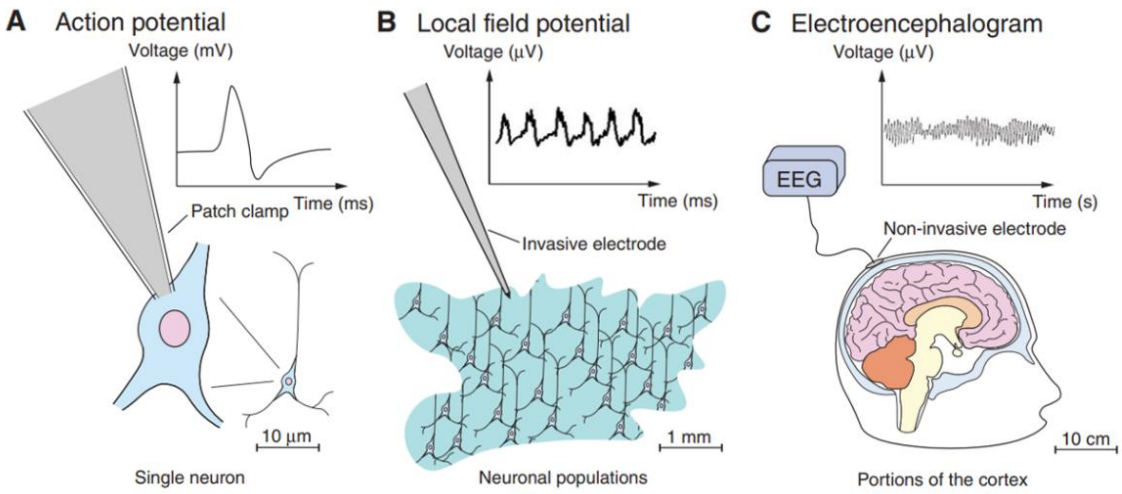

Figure 2.2*: Schematization of the EEG. [A] An action potential is generated by a single neuron. [B] Several neurons together form a neuronal population which will create a local field potential. [C] This local field potential will be recorded using non-invasive electrodes, allowing the creation of the electroencephalographic signals. Retrieved from* (Biasiucci et al., 2019).

2.1.4. Types of Electrodes

Electrodes placed over the scalp are used in order to obtain the activity of the neurons in a non-invasive way. The set of neural activity obtained from the group of used electrodes is called electroencephalogram.

Electrodes can be divided into dry or wet – use of fluids – and active or passive – electrical amplification type. They are classified into dry if they do not require a saline solution or electrolytic gel and wet if they do. As for electrical amplification type classification, the primary difference is that active

electrodes amplify the EEG at the scalp, while on the contrary passive electrodes amplify the EEG in the (pre)amplifier at the electrode wire's end (*EEG ELECTRODES*, 2017).

Wet electrodes are the most commonly used. They consist in small discs of silver and silver chloride (Di Flumeri et al., 2019) that are placed under the scalp (Shad et al., 2020). Some attributes of silver chloride are the reason to use it as preferable material to build electrodes: silver chloride has a low solubility in water – saturates quickly, reaching an equilibrium point just as quickly (Di Flumeri et al., 2019).

Regarding dry electrodes they are based on microelectromechanical systems (MEMS), with the electrode acting as a conductor between the skin and the electrode itself. Normally, stainless steel is used for this type of electrodes (Cionek, 2020; Lopez-Gordo et al., 2014).

Active electrodes have a co-integrated amplifier that is responsible for reducing noise by minimizing the distance between the electrode and the amplifier (Xu et al., 2017).

Regarding passive electrodes, these do not contain any amplifier. Their function is only to extend the connection of the conductive material to the equipment to record, process or amplify the signal (Cionek, 2020).

As for wet electrodes, the amplitude signal coming from them is very attenuated, since there are some anatomical structures, namely the scalp (represented in **Figure 2.3**), which make the signal reception weak. Besides this, the air electrical conductivity is approximately zero, being necessary a sort of bridge to connect the scalp and the electrodes (Cohen, 2014). Thus, it is necessary to resort to some techniques, namely the application of electrolytic gel or saline solution. This is why they are called wet electrodes.

Regarding the application of the conductive electrolyte substance to the wet electrodes, the use of saline solution turns out to be less time-consuming compared to the application of electrolyte gels, as the saline solution spreads quickly over the scalp. However, it may create unwanted short circuits between electrodes (*The Wet-EEG Cap: Semi-Dry, Saline & Gel EEG Caps | Bitbrain*, 2018).

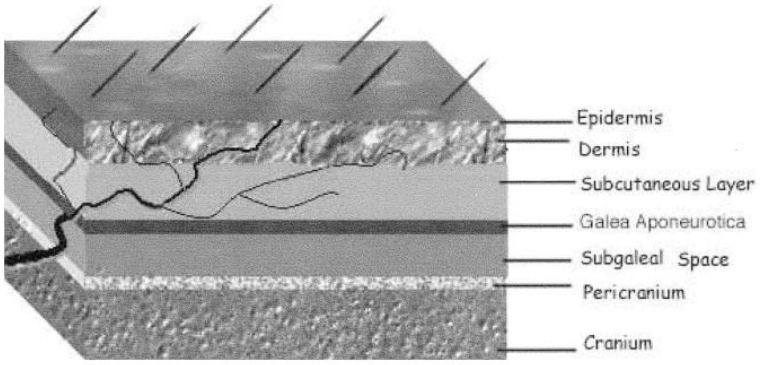

Figure 2.3*: The various layers of the scalp. From the most superficial to the innermost, there are: epidermis (commonly known as skin), dermis, subcutaneous layer, aponeurotic galea, subgaleal space, pericranium and cranium. Retrieved from* (Seery, 2002).

2.1.5. Electrode Location

2.1.5.1. International 10-20 System

In order to standardize the electrodes positions throughout the world, the *International 10-20 System* (Morley et al., 2016) was created. This system is based on the relationship between the location of the electrode and the area of the underlying cerebral cortex.

The numbers 10 and 20 refer to the fact that the distance between adjacent electrodes is 10% or 20% of the total inion-nasion distance or LP-RP (*The 10-20 System for EEG - Electrophysiological Research Blog, News & Events - TMSi*, 2022), as explained in **Figure 2.4**. Consequently, the inter-electrode space is equal and the positioning of the electrodes is customisable to each individual (Morley et al., 2016).

The inion, nasion, RP and LP are reference points on the scalp for the EEG. Thus, they are used to discover the position of *Cz*. The location of the *Cz* is given by the intersection of the inion-nasion and RP-LP lines.

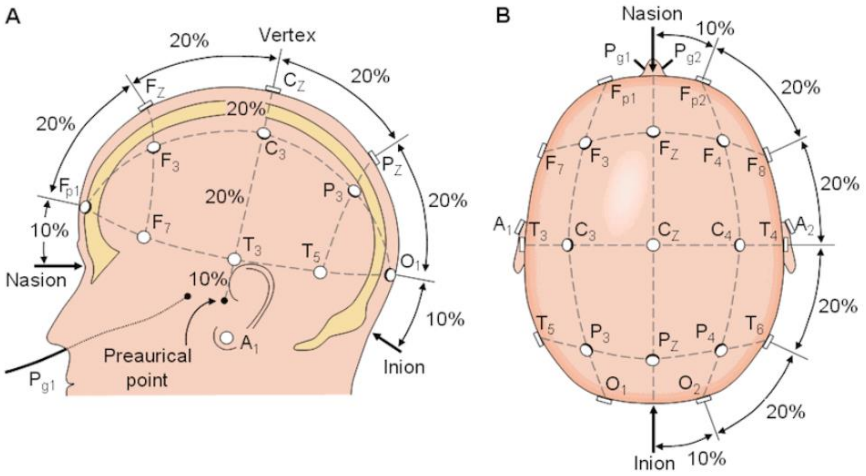

***Figure 2.4**: The 10-20 system and its distances. [A] Sagittal plane. [B] Transverse plane. Retrieved from (The 10-20 System for EEG - Electrophysiological Research Blog, News & Events - TMSi, 2022).*

The electrodes cover all brain regions: temporal cortex (T), parietal cortex (P), occipital cortex (O) and frontal cortex (F). Therefore, the first letter of each electrode corresponds to the location of the cortex under which it is located. Following the first letter, there is a number or a second letter. Odd numbers are used for the left hemisphere of the brain, even numbers for the right. If the electrode is located under the midline, it receives the letter z. **Figure 2.5** is an example of a 16-channel EEG with the nomenclature of the respective electrodes.

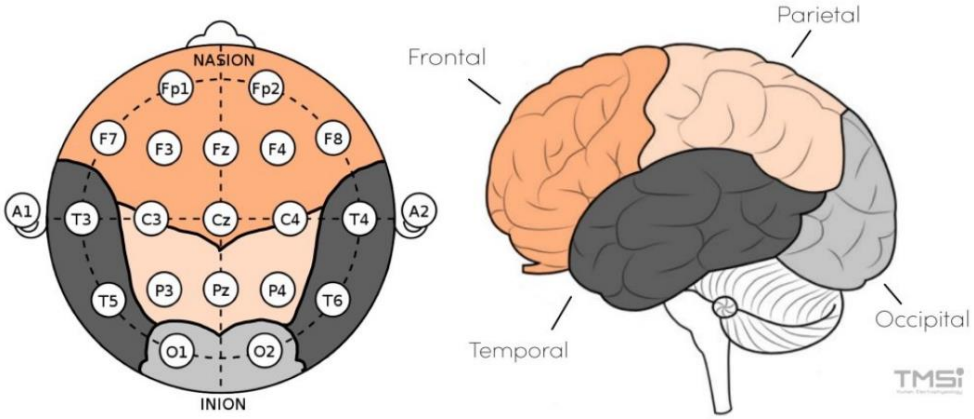

***Figure 2.5**: Electrode positioning and respective nomenclature of a 16-channel EEG, as well as the correspondence of brain regions, according to the International 10-20 System standards. Adapted from (The 10-20 System for EEG - Electrophysiological Research Blog, News & Events - TMSi, 2022).*

2.1.5.2. EEG Caps

There are EEG caps with various sizes and electrode placement labels available. Depending on the supplier, some caps have the electrodes built in – EGI (Electrical Geodesics, Inc), the provider for FMUL (Faculdade de Medicina da Universidade de Lisboa), is one of these –, while the electrodes may be removable from other caps.

It is also important to note the importance of choosing a cap of adequate size for the subject, according to the head circumference. This is because, if the cap is too big, the electrodes may not be in contact with the scalp; if the cap is too small, it may cause discomfort for the subject.

To obtain real EEG signals from each brain area, it is necessary that the electrodes are positioned in the correct place under the scalp, as well as that the *Cz* is at the intersection between the nasion-inion and LP-RP distances (*The 10-20 System for EEG - Electrophysiological Research Blog, News & Events - TMSi,* 2022). Otherwise, if the labelled electrode is not placed where it belongs, the electrode will not correspond to the expected region of the brain.

2.1.5.3. Geodesic

A geodesic system is a technique for calculating an object's position inside a geometric space. Based on the available sensor data and environmental restrictions, geodesic systems in localization frequently use mathematical models and algorithms to identify the most likely location of an object.

High-density EEG is now a reality thanks to EGI's cutting-edge Geodesic EEG System (GES) solutions, which feature simple-to-use sensors, clear software, and a modular product structure that may fit any facility. The Geodesic system provided by EGI (and other systems) allows to store the electrode locations in cartesian and spherical coordinates (*Electrical Geodesics, Inc.*, 2021).

2.1.6. High Density EEG

High-density EEG (HD-EEG) has emerged to make up for the lack of spatial resolution that traditional EEG presents. Therefore, there is greater precision in the location of the origin of the signal, as well as more accurate mapping of brain functions (Dattola et al., 2020).

HD-EEG differs from conventional EEGs, in technical terms, by the larger number of channels, usually 128 or 256 (*High-Density Electroencephalogram (HD-EEG) on Epilepsy and Tumor - Clinical Trials Registry - ICH GCP*, 2023).

This type of EEG is closely associated with MRI, as it allows for a localisation of the source of the signals that is customisable to each individual, meaning that source reconstruction uncertainty is reduced in HD-EEG (*High-Density Electroencephalogram (HD-EEG) on Epilepsy and Tumor - Clinical Trials Registry - ICH GCP*, 2023).

2.1.7. EEG Rhythms

EEG signals can contain several types of frequencies, ranging from slow frequencies (<0.01 Hz) to ultra-fast frequencies (>1000 Hz). Fast waves reside in a limited neural volume, unlike slow waves that are usually accompanied by large synchronous membrane voltage fluctuations in massive brain regions (Buskila et al., 2019). However, the conventional bandwidth of clinical EEG is 0.5 Hz to 30 Hz (Nayak & Anilkumar, 2020).

EEG rhythms – also called EEG waveforms or brain waves – refer to brain wave activity associated with specific frequency bands. EEG rhythms represent clusters of neural oscillations that function as distinct units during specific brain functions associated with different types of activity. For example, some are related to sleep, others to states of consciousness and wakefulness. Thus, EEG rhythms serve as tools for brain research and clinical diagnostics (Buskila et al., 2019).

The main EEG rhythms are: delta (δ), theta (θ), alpha (α), beta (β) and gamma (γ). Despite the fact that there is not a consensus in the literature about which frequencies correspond to each EEG rhythm, commonly they are assigned as (Buskila et al., 2019; Cole & Voytek, 2017):

- Delta: 1-4 Hz;
- Theta: 4-8 Hz;
- Alpha: 8-12 Hz;
- Beta: 12-30 Hz;
- Gamma: >30 Hz.

Regarding the delta rhythm, it can be found in the neocortex (the most superficial layer of the cerebrum), thalamus and basal ganglia. Delta wave is predominant in many brain functions, such as: slow frequency waves and deep NREM sleeps; decision making; concentration, focused attention and motivation; memory reinforcement; and facilitating layer interconnections to control synaptic rescaling in the cortex (Buskila et al., 2019; Cole & Voytek, 2017).

As for the theta wave, it is more accentuated in the hippocampus, cortex, amygdala and dentate gyrus. Its main brain functions correspond to: REM sleep; selective attention, arousal, orientation, and voluntary movement control; modulation of synaptic strength and coordination of active neuronal

populations phase-encoding; and episodic memory, environmental encoding, and word processing (Buskila et al., 2019; Cole & Voytek, 2017).

Furthermore, there is the alpha rhythm that is predominant in the neocortex and thalamus. This is one of the most important brain waves when talking about cognition. Besides this, its brain functions include: drowsiness and calm state; sensorial functions, framing visual concepts and movement; working memory and task engagement; motor imagery (mental execution of a movement); and visual stimuli and reaction in the occipital lobe (Buskila et al., 2019; Cole & Voytek, 2017; Hohaia et al., 2022).

Regarding the beta wave, it is mostly found in the neocortex, olfactory bulb, thalamus, hippocampus and striatum. This rhythm is predominant in the following brain functions: motor preparation and sensorimotor control; amplification of sensory processing of visual and olfactory stimuli; earmarking of working memory; and motor imagery and execution (Buskila et al., 2019; Cole & Voytek, 2017; McFarland et al., 2000).

Finally, the gamma rhythm. This is mostly present in the neocortex, olfactory bulb, and hippocampus. Its main brain functions correspond to: motor task involvement and focused attention; evoked auditory and visual stimuli processing; recognition memory and spatial working; and cognitive processing (Buskila et al., 2019; Cole & Voytek, 2017).

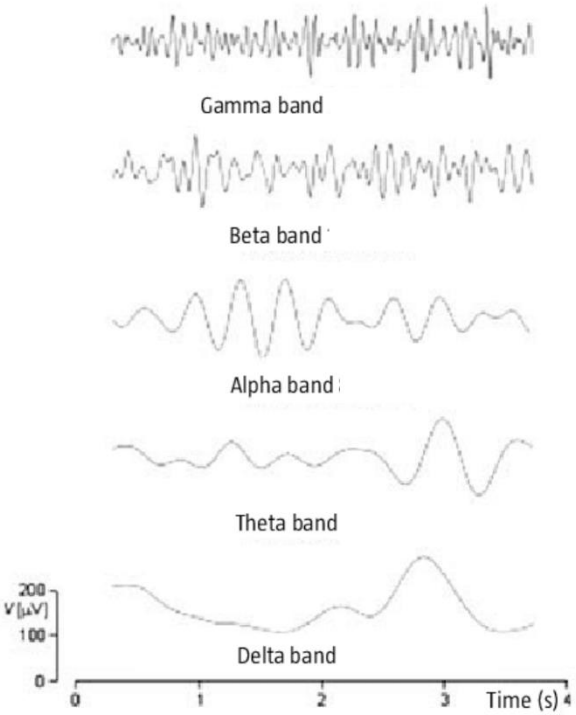

***Figure 2.6**: Representation of EEG traces for the brain oscillations: delta, theta, alpha, beta and gamma. Adapted from* (Lattari et al., 2010).

To sum up, **Table 1** describes the brain areas and functions for each EEG rhythm.

***Table 1**: EEG rhythms summary.*

EEG Rhythm	Brain Area	Brain Function	References
Delta (1-4 Hz)	Neocortex, Thalamus, Basal ganglia.	NREM sleep, Decision making, Concentration, Attention and motivation, Memory reinforcement.	(Buskila et al., 2019; Cole & Voytek, 2017).
Theta (4-8 Hz)	Hippocampus, Cortex, Amygdala, Dentate Gyrus.	REM sleep, Selective attention, Arousal, Orientation, Voluntary movement control, Episodic memory, Environmental encoding, Word processing.	(Buskila et al., 2019; Cole & Voytek, 2017)
Alpha (8-12 Hz)	Neocortex, Thalamus.	Cognition, Drowsiness and calm state, Sensorial functions, Framing visual concepts and movement, Working memory and task engagement, Motor imagery, Visual stimuli processing.	(Buskila et al., 2019; Cole & Voytek, 2017; Hohaia et al., 2022)
Beta (12-30 Hz)	Neocortex, Olfactory bulb, Thalamus, Hippocampus, Striatum.	Motor preparation and sensorimotor control, Amplification of sensory processing of olfactory and visual stimuli, Earmarking of working memory, Motor imagery and execution.	(Buskila et al., 2019; Cole & Voytek, 2017; McFarland et al., 2000)
Gamma (>30 Hz)	Neocortex, Olfactory bulb, Thalamus, Hippocampus, Striatum.	Motor task involvement and focused attention, Evoked auditory and visual stimuli processing, Recognition memory and spatial working, Cognitive processing.	(Buskila et al., 2019; Cole & Voytek, 2017)

These EEG signals carry three fundamental pieces of information (Cohen, 2014): frequency, that measures how fast the signal is going; power, which is linked to the amplitude of the signal; and, phase, that indicates the temporal location. These concepts will be approached deeper in the next chapters. It is important to note that EEG signal contains a set of frequencies, being then common to associate to a frequency band.

2.1.8. Event-Related Potentials

Event related potentials (ERPs) are variations in brain activity created by a certain (or multiple) event, such as stimuli, decisions and responses (Luck, 2012). ERPs have been a great concept of interest because of their potential to disclose how cognitive processes work (Bressler & Ding, 2006).

The positive and negative wavelike components that make up the ERP waveform are distinguished by their occurrence times and polarities (Bressler & Ding, 2006). Thus, to identify when the ERP occurred, it is normally used the notation 'N' (negative) or 'P' (positive), to mark that the ERP occurred at the negative or positive peak of the wave; and the letter if followed by a number which marks the time moment. For instance, an ERP 'N200' occurred as a negative wave that peaks 200 ms after the event (Bressler & Ding, 2006).

There are three types of event-related potentials: sensory, that may be evoked by an external stimulus that reaches the person through their sensory organs; motor, that might be evoked through a movement-related event; and cognitive, that are related to cognitive functions (Bressler & Ding, 2006).

To analyse ERPs in multiple trials, the mathematical basis is: sum the voltage at each time point over the trials and divide by the number of trials, meaning a mathematical mean. This is explicit in **Figure 2.7**.

The ERPs' responses can be quantified using event-related desynchronization/synchronization method. Basically, a decrease in power of a frequency during the event processing – compared to a baseline – is known as event-related desynchronization (ERD). The reverse process in which there is an increase in power is known as event-related synchronization (ERS) (Pfurtscheller & Da Silva, 1999). Thus, within-subject assessments of relative changes in the EEG are represented by the ERD/ERS values (Pfurtscheller & Da Silva, 1999).

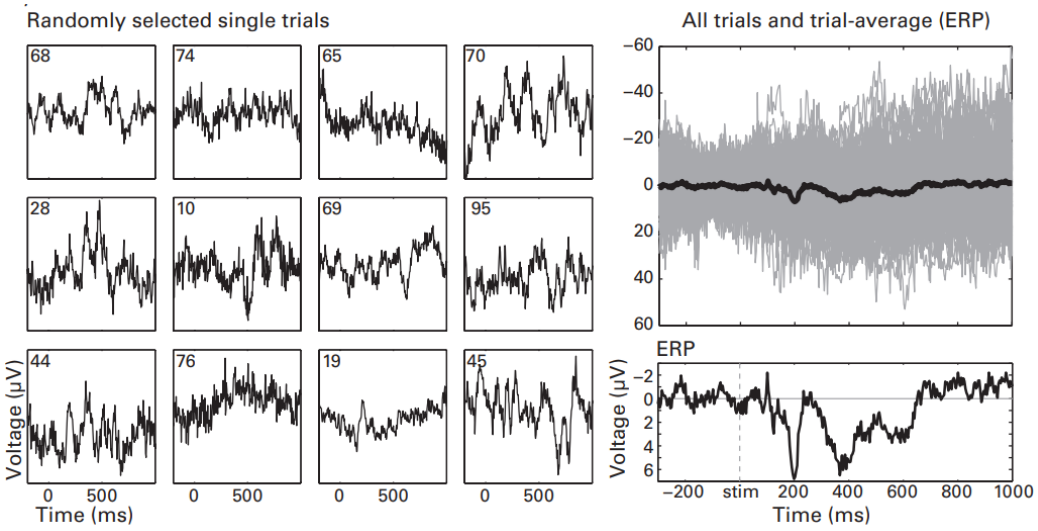

***Figure 2.7**: The left part represents the EEG traces from 12 different trials, from electrode FCz. The right upper graphic shows 99 trials (in grey) and their average. The right lower graphic shows the average ERP. Retrieved from (Pfurtscheller & Da Silva, 1999).*

The power difference between the signal of interest after the event ('*A*') and the baseline signal ('*R*'), whether it is in the time domain or frequency domain, must be known in order to calculate ERD/ERS. With this, the mathematical expression is quite simple (Kalcher & Pfurtscheller, 1995), as seen in **Equation 1**:

$$ERD\ (\%) = \frac{R - A}{R} \times 100$$

***Equation 1**: ERD formula.*

2.2. Magnetic Resonance Imaging

MRI is a neuroimaging tool that has been widely used during the last years. In addition to the fact that full brain coverage and not requiring ionizing radiation, MRI also has a great spatial resolution (1 mm) (Oldendorf et al., 1988).

2.2.1. How does Magnetic Resonance Imaging Work?

MRI uses the magnetic properties of the human body to construct an image. This is due to the fact that there is a large percentage of water molecules and fat matter, which makes for a fairly significant amount of hydrogen nuclei in the human body (Berger, 2002).

When the hydrogen protons are under an external magnetic field, B_0, they will orient themselves according to its direction, with a part of them in the parallel direction and another part in the antiparallel direction to the applied magnetic field. During this process, the magnetization vector is created, with direction and orientation of $\overrightarrow{B_0}$. This magnetization vector has only one longitudinal component (B_0) (Berger, 2002).

To understand how MRI works, it is imperative to pay attention to the following equation, in which γ is the gyromagnetic ratio, a constant specific to each particular nucleus or particle:

$$f_0 = \gamma B_0$$

***Equation 2**: Larmor equation*

A radio frequency (RF) pulse is applied at Larmor frequency, f_0 which results in a new magnetic field, B_1. RF pulses are used in MRI to temporarily disrupt the magnetic field of hydrogen atoms inside the body, allowing the machine to detect those signals and create detailed images of internal structures. By applying the RF pulse, the longitudinal magnetization is transformed into a transverse one. Shortly after this phenomenon happens, the magnetization vector returns again to its longitudinal component, which causes the emission of energy. This event previously described is known as relaxation, which is subsequently translated into the free induction decay (FID) – the signal that will allow the reconstruction of the desired image (Berger, 2002; Westbrook & Talbot, 2018). The FID corresponds to the change in flux caused by the precession of the transverse magnetization.

2.2.2. MRI Time Parameters

The relaxation phenomenon implies some relevant times definitions (Westbrook & Talbot, 2018):

- **T1**: Time, normally in milliseconds (ms), that hydrogen nuclei need to return to 63% of the longitudinal magnetization value;
- **T2**: Time, usually in milliseconds (ms), that hydrogen nuclei need to lose 63% of the transverse magnetization value;
- **TE**: Time, usually in milliseconds (ms), between delivering the RF pulse and receiving the echo signal (reorientation of spin magnetization by a pulse of resonant electromagnetic radiation);

- **TR**: Time, normally in milliseconds (ms), between successive pulses applied to the same slice.

The various tissues of the human body have different T1 and T2, which results in organs with distinct contrasts. In this way, this property allows to inspect certain organs of the body by MRI imaging.

2.2.3. Equipment

The MRI device consist of four main components (Serai et al., 2021), shown in **Figure 2.8** and **Figure 2.9**:

- **Magnet**: Composed of superconducting coils that form a giant magnet. Usually, the magnet field is 1.5T or 3T;
- **Gradient coil**: They are used for the spatial coding of the MRI signal, providing information about the spatial location of the hydrogen atoms in the human body;
- **RF coil**: They are responsible for emitting the RF pulses and receiving the signal emitted by the subject. They should be placed so that the B_0 and B_1 fields are perpendicular;
- **Computer software**: This has several functions, namely to control the RF and gradient pulses, receive the data and display the images created.

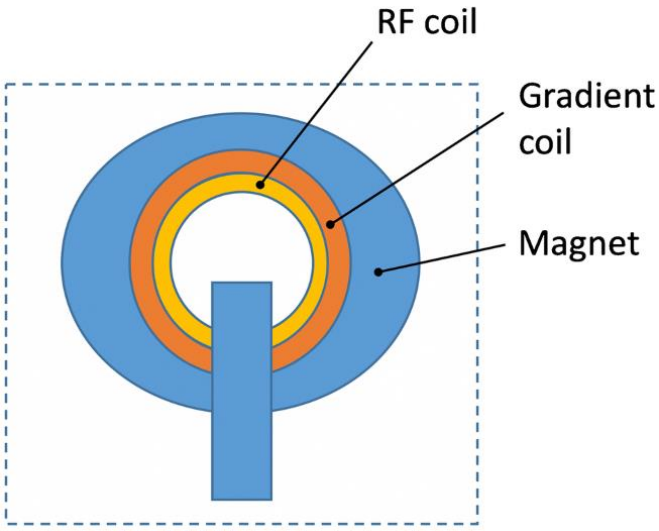

***Figure 2.8**: MRI components - magnet, gradient coils and RF coils. The figure does not show the computer system. Retrieved from* (Serai et al., 2021).

***Figure 2.9**: Philips MRI Ingenia Elition 3.0 T. Retrieved from* (MR Ingenia Elition 3.0T | Philips, 2023).

2.2.4. Functional Magnetic Resonance Imaging

Functional magnetic resonance imaging (fMRI) is currently among the most widely used methods in neuroscience and cognitive sciences (Logothetis, 2008).

To preform fMRI it is needed T2* (T2 weighted image) contrast. The first T2 can be regarded as the "natural" or "true" T2 of the tissue being scanned, whereas T2* can be considered a "observed" or "effective" T2 (*T2* vs T2 Relaxation Time - Questions and Answers in MRI*, 2023).

Brain activity is related to aerobic metabolism. This means that when a certain brain region is more active, there is a greater oxygen input in that area. As such, fMRI uses the BOLD (Blood-Oxygen-Level-Dependent) contrast mechanism that measures oxygen concentration, being the source of signal the paramagnetic deoxyhemoglobin (Logothetis, 2008; Westbrook & Talbot, 2018).

To obtain a brain activation image, it is sufficient to subtract the MRI image obtained at the onset of a certain stimulus from the MRI image initially obtained without any stimulus. It is important to note the poor temporal resolution and the great spatial resolution.

In terms of equipment, there is no difference between MRI and fMRI. The only distinction lies in the software available in the computer system (Holdsworth & Bammer, 2008).

2.3. EEG-fMRI

2.3.1. History and Importance

EEG was discovered about seven decades ago and fMRI about two decades ago. Since then, both have been used separately. However, more than two decades ago, it began to work as symbiosis method (Ritter & Villringer, 2006), meaning that we could have the best of both worlds at the same time: we have

the spatial resolution of the fMRI and, furthermore, the time resolution of the EEG (Rosenkranz & Lemieux, 2010).

The first experiments involving EEG-fMRI are dated 1993 when researchers were studying epilepsy. They intended to get a better spatial resolution of the epileptic networks (Jorge et al., 2014).

EEG-fMRI has several applications, such as: diagnostic and pre-surgical planning. This is also a powerful tool for neuroscience and cognitive studies, making possible the analysis of spontaneous brain activity (Rosenkranz & Lemieux, 2010).

2.3.2. The Technique

The equipment used to perform EEG-fMRI is essentially the same as performing EEG and fMRI separately, with one clear and important point: the EEG equipment should be MRI compatible.

2.3.3. Artifacts

EEG-fMRI is a recently used technique due to the several problems that the combination of these two worlds brings. Over the years, the equipment has been improved to reduce the inherit noise effects between MRI and EEG. One of the main problems is the creation of an electromotive force due to the presence of an electric circuit in high magnetic field (Ritter & Villringer, 2006).

The main four artifacts that appear in the EEG when using it inside the MRI are: ballistocardiogram (BCG), MRI gradient artifact, motion artifact and environmental artifact (Hargreaves et al., 2011).

The first one appears due to the cardio-respiratory sequences, meaning, it captures the cardiac ballistic forces caused by the sudden discharge of blood into the great vessels with each heartbeat, breath, and body movement. This is amplified by the MRI.

Gradient artifact which are caused by magnetic field gradients that cause currents in EEG electrodes that are up to 400 times larger than cerebral activity and obfuscate EEG information, are the main source of noise in EEG fMRI (Hargreaves et al., 2011).

The motion artifact happens as a consequence of the subject's movement, which will induce current when inside the MRI scanner (Hargreaves et al., 2011). This happens because, according to the Faraday law, the moving body acts like a conductor, causing changes in the magnetic field.

Finally, the environmental noise occurs because of external factors, highlighting the 50 Hz noise that is due to the power supply (this frequency is applied to Europe, Africa, Asia, Australia and some South American countries). There are other factors, such as: lights in MRI room and ventilation (Hargreaves et al., 2011).

2.4. Neuroanatomy

In this section, it will be described the brain anatomy, in general. This because some of the brain regions described will be of particular interest to perform the data analysis.

2.4.1. Human Brain

The human brain is the command centre of the nervous system, being responsible for interpreting outside information (*Human Brain: Facts, Functions & Anatomy | Live Science*, 2021). Besides this, it controls memory, speech, thoughts, body parts' movement and the function of many organs, as well as non-volitional functions, such as: breathing, digestion, temperature regulation, heart beating, etc (*Brain Anatomy, Anatomy of the Human Brain | Mayfield Brain & Spine Cincinnati, Ohio*, 2018). The human brain is divided in three parts: cerebrum, cerebellum and brainstem, as shown in **Figure 2.10**. However, it is important to keep in mind that many times people refer to the cerebrum as brain.

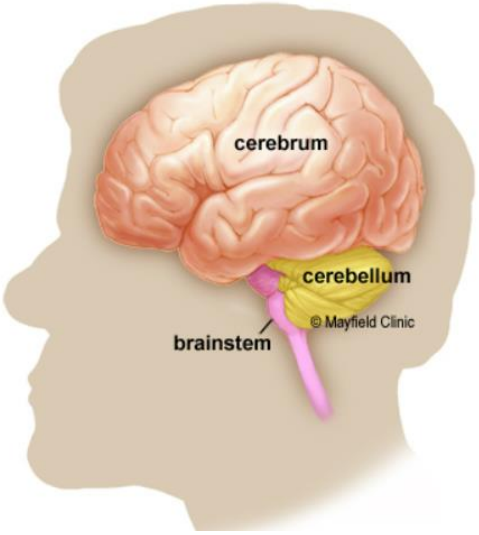

***Figure 2.10**: The main parts of the cerebrum: cerebrum, brainstem and cerebellum. Retrieved from. Retrieved from (Brain Anatomy, Anatomy of the Human Brain | Mayfield Brain & Spine Cincinnati, Ohio, 2018)*

The cerebrum is the largest part and it is divided in two hemispheres – left and right hemispheres. Besides, the cerebrum is responsible for higher functions, like emotions, speech and motor activity. The cerebellum is right under the cerebrum and it is responsible for muscle movements, maintaining posture and balance. The brainstem connects cerebrum and cerebellum to the spinal cord and is responsible for automatic functions, for example breathing and body temperature (*Brain Anatomy, Anatomy of the Human Brain | Mayfield Brain & Spine Cincinnati, Ohio*, 2018).

Particularly, the cerebrum is divided into lobes. Traditionally, there were four lobes: frontal, parietal, temporal and occipital, but up today two more lobes were considered: the insular and limbic lobes (*Cerebral Cortex: Structure and Functions | Kenhub*, 2023), as illustrated in **Figure 2.11**.

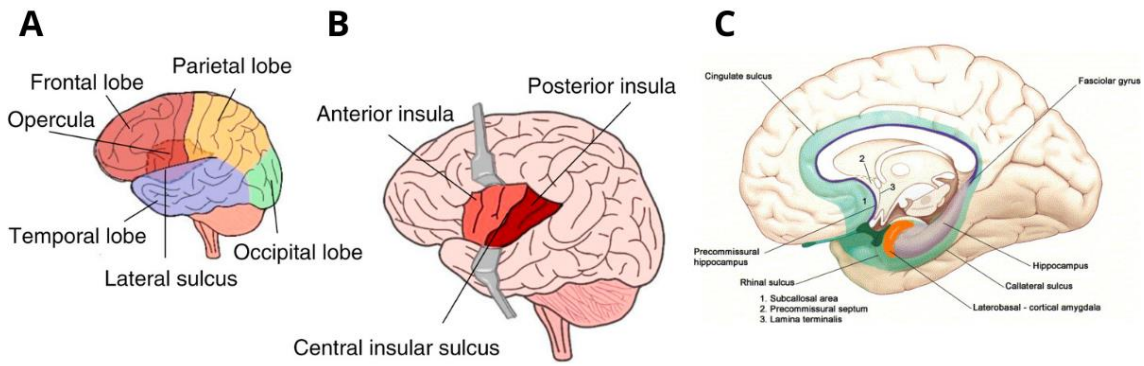

***Figure 2.11**: [A] Schematic representation of the main brain lobes: frontal (red), temporal (purple), parietal (yellow) and occipital (green); [B] insular lobe (red); [C] limbic lobe (green). Adapted from (Gogolla, 2017; Heimer & Van Hoesen, 2006).*

The frontal lobe is linked to attention, short term memory tasks, control of voluntary movement and motivation. The parietal lobe integrates mechanoreceptor stimuli and proprioceptive, involved in language mechanism. The temporal lobe function is to decode sensory inputs into derived meanings for language comprehension and retention of visual memory. Finally, the occipital lobe is responsible for visual processing (*Cerebral Cortex: Structure and Functions | Kenhub*, 2023). The insular lobe is located inside the lateral sulcus – a deep fissure in each hemisphere that separates the temporal lobe from the parietal and frontal lobes of each hemisphere – and its function is to process and integrate the taste sensation, visceral and pain sensation and some vestibular functions (Gogolla, 2017). The limbic lobe is located at the inferomedial aspect of the cerebral hemispheres and consists of two concentric gyri – ridge on the brain surface – surrounding the corpus callosum – a large tract that connects the two hemispheres of the brain (Rajmohan & Mohandas, 2007). The limbic lobe functions are: modulation of visceral and autonomic functions, learning, modulation of emotions and memory.

2.4.2. Brodmann Areas

Korbinian Brodmann was a famous German neurologist who divided the human brain in several areas, the so called Brodmann areas (Strotzer, 2009).

Brodmann classified the cerebral cortex's 52 separate regions. Despite having cytoarchitectural traits that were noticeably distinct, Brodmann frequently discovered ill-defined boundaries between the zones (Strotzer, 2009). It is crucial to understand that the boundaries between the areas frequently do not line up perfectly with the sulci (Strotzer, 2009). These 52 areas are represented in **Figure 2.12**.

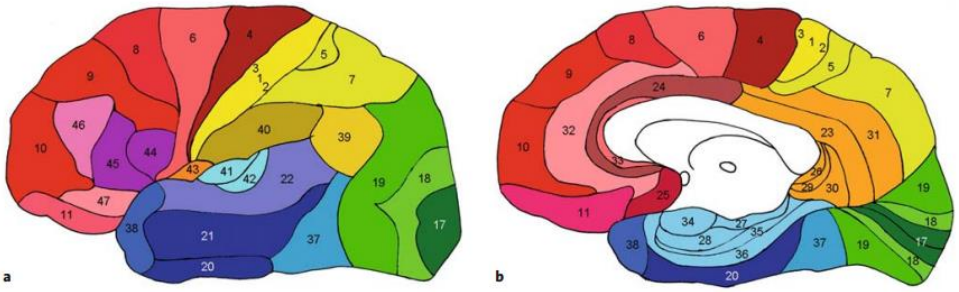

***Figure 2.12**: Schematic representation of Brodmann areas. [A] Lateral view. [B] Medial surface view. Retrieved from* (Strotzer, 2009).

2.4.3. Nucleus Accumbens

Commonly, nucleus accumbens (NAc) is associated with pleasure, emotional and motivational processes, the limbic-motor interface, motivational and dependence mechanisms, and the effects of particular types of psychoactive drugs (Pereira & Neto, 2014; Salgado & Kaplitt, 2015). Besides, nucleus accumbens is implicated in several neuropsychiatric disorders, such as: Alzheimer's disease, anxiety, Parkinson's disease, depression, bipolar disorder, obesity, Huntington's disease and addiction (Salgado & Kaplitt, 2015). Recently, some cientists discovered that NAc is integrated in rewarding circuits in human brain (Pereira & Neto, 2014). NAc is often referred to as the "pleasure centre" (Pereira & Neto, 2014).

Nucleus accumbens is located in front of the posterior border of the anterior commissure (AC) and parallel to the midline. Its delimitations have been not clear, but according to (Salgado & Kaplitt, 2015), its boundaries includes several structures, such as the internal capsule and the lateral ventricle. The location of the NAc is represented in **Figure 2.13**.

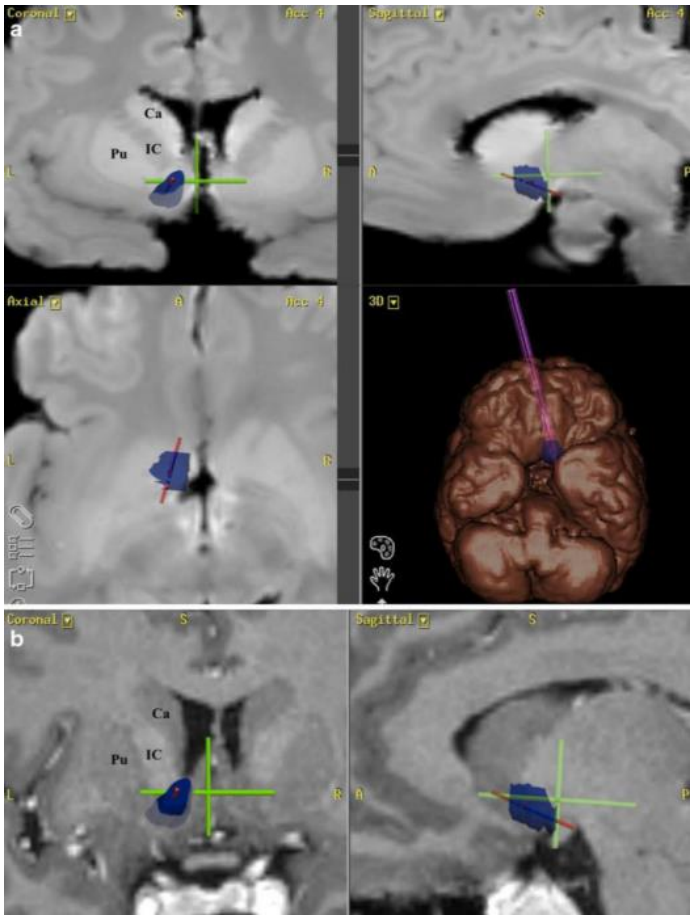

***Figure 2.13**: The location of nucleus accumbens (blue), in vivo, obtained with a MRI scanner. It is visible the three planes – coronal, sagittal and axial – as well as a 3D model. Retrieved from (Pereira & Neto, 2014).*

Regarding the EEG signal from NAc, it can be easily measured invasively. Despite this, when using non-invasive EEG, source reconstruction can be used to measure EEG electrical activity from NAc (Wacker et al., 2009).

2.4.4. Medial Prefrontal Cortex

The medial prefrontal cortex (mPFC) is widely studied in experiments involving decision making, executive control, conflict monitoring, error detection, reward-guided learning and decision making about risk and reward (Euston et al., 2012), being this informed by MRI studies.

According to (Alexander & Brown, 2011), mPFC can be an important piece when formatting expectations about actions and detecting extraordinary outcomes. Other research works state that the mPFC should learn to predict value of action (Alexander & Brown, 2011).

When a person is presented to emotional stimuli, there are a few brain areas activated, more concretely, the medial prefrontal cortex (Etkin et al., 2011). This shows that mPFC might be one of the areas responsible for emotional processing. Additionally, recent studies suggest that the medial prefrontal cortex has important regulatory roles in many cognitive functions, such as: attention, inhibitory control, spatial memory and long-term memory (Jobson et al., 2021).

Medial prefrontal cortex is located at the front part of the frontal cortex, as represented in **Figure 2.14**.

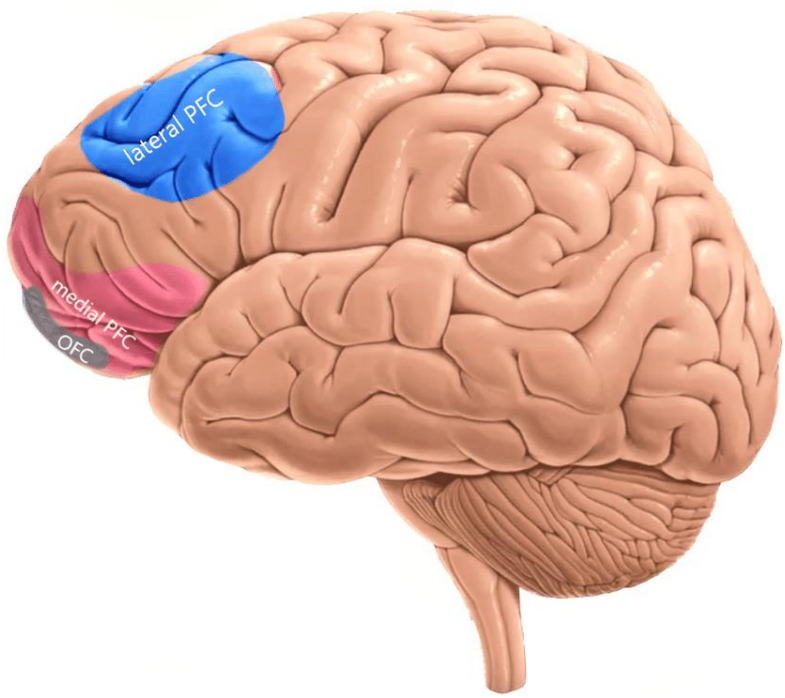

***Figure 2.14**: Schematic representation of the location of the medial prefrontal cortex (mPFC), in pink. Adapted from (Salehinejad et al., 2021).*

2.4.5. Anterior Cingulate Cortex

Anterior cingulate cortex (ACC) is a brain region that belongs to the limbic system (Bush et al., 2000). According to (Bush et al., 2000), there are three points that every researcher should have in mind when studying the ACC: first, the cingulate cortex contains particular processing modules for sensory, cognitive, motor and emotional information; second, the cingulate cortex integrates input from a variety of sources, such as motivation, error assessment, representation of cognitive and emotional networks; third, ACC influences brain activity in others brain regions and regulates motor, cognitive, visceral and endocrine responses. Recent studies suggest that the ACC is also linked to the decision-making process and conflict monitoring – which means the detection of when two competing choices might be made during a certain task (Kolling et al., 2016).

It is important to note that the cognitive and emotional information is processed separately in ACC. Therefore, anterior cingulate cortex can be divided in two parts: dorsal cognitive division (ACcd) which is represented by areas 24b'-c' and 32' in **Figure 2.15** and rostral–ventral affective division (ACad) which is illustrated by areas 24a-c, 25, 32 and 33 in **Figure 2.15**.

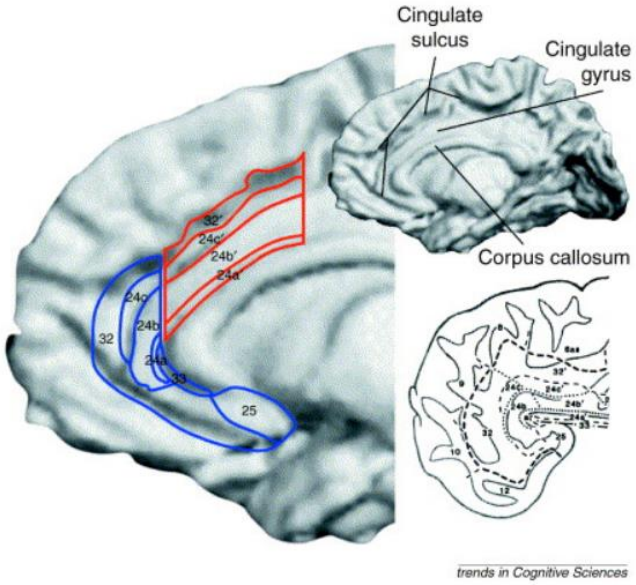

***Figure 2.15**: Anterior cingulate cortex anatomy via MRI. On the left parti is represented the cytoarchitectural areas of anterior cingulate cortex, highlighting the cognitive part in red and the affective in blue. On the bottom right corner it is shown a scheme of the ACC areas. Retrieved from* (Bush et al., 2000).

2.5. EEG Processing and Pre-Processing Methods

2.5.1. Independent Component Analysis (ICA)

To start explaining independent component analysis (ICA) is often recurred to the cocktail-party problem (Hyvärinen et al., 2001). Imagining that there are three people in a room talking simultaneously and three microphones recording in different spots of the room, these signals recorded from each microphone will be the sum of three people signals. What ICA does is estimate the original speech signals (Hyvärinen et al., 2001).

Technically, ICA is a source separation technique responsible for decomposing the mixed EEG signals into components to find independent sources of data variation (Cohen, 2014). ICA can be used with two purposes: clean EEG data or data dimension reduction technique (Cohen, 2014). When used as a pre-processing tool, the goal is to reject components that contain artifacts, based on their frequency spectra, topographies and time courses (Cohen, 2014).

It is important to have in mind that ICA is based on statistical characteristics, meaning that ICA cannot label that one component is purely noise or purely signal (Cohen, 2014). Components are likely to have both, but it is important to set a threshold, making easier to choose which components to remove from the data.

The maximum number of components that can be generated is equal to the number of active electrodes (Cohen, 2014), which excludes the reference and the ECG. This leads to a maximum number of 256.

2.5.2. Time-Frequency Analysis

EEG data reflects brain activity, which is a result of the EEG rhythms. These EEG rhythms contains several frequencies at the same time that can be separated. Perceptual, cognitive, physical, linguistic, social, emotional, mnemonic, and other functional processes all change rhythmically in response to a certain type of task (Cohen, 2014). To perceive these changes in brain activity, it is important to analyse how the frequency bands change over time, using for that time-frequency analysis (Qian & Chen, 1999).

The way to visualize data in time-frequency domain can be perceived in a 3D way, being the dimensions: time, frequency and other feature on the z-axis, such as power (Cohen, 2014).

2.5.2.1. Time-Frequency Methods

To perform time-frequency analysis, there are several signal processing methods (Al-Fahoum & Al-Fraihat, 2014) such as: Short-Time Fourier Transform (STFT), Continuous Wavelet Transform (CWT), Wigner-Ville Distribution (WVD) and Wavelet Packet Transform (WPT). Let's take a look at the first two (STFT and CWT), since both are used in the present dissertation.

2.5.2.1.1. Short Time Fourier Transform (STFT)

Short-time Fourier Transform (SFTF) consists of a series of Fourier transforms of a windowed signal. When the frequency of signal changes over time, the SFTF gives time-localized frequency information, whereas the conventional FT produces an averaged frequency information across the whole signal time interval (Lu et al., 2018). This process is illustrated in **Figure 2.16**.

In STFT, the resolution of time and frequency can be seen as a trade-off. To put it in another way, a narrow-width window generates a good resolution in the time domain, but a poorer resolution in the frequency domain, and vice-versa (Lu et al., 2018).

One of the most commons ways used to visualize STFT is through spectrogram, which is an intensity representation of SFTF magnitude over time in a 2D plot (Chaurasiya, 2020; Lu et al., 2018).

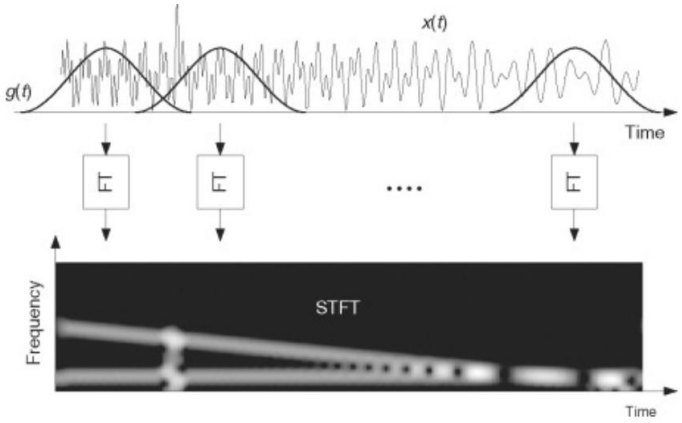

***Figure 2.16**: Representation of short-time Fourier transform.*

2.5.2.1.2. Continuous Wavelet Transform (CWT)

Wavelet analysis allows the estimation of a time series' spectral properties as a function of time, which exposes changes in periodic components over time (Aguiar-Conraria & Soares, 2014). Wavelet transform (WT) is very important in diagnosis, because it compresses the biomedical signal into few parameters that represents the signal (Al-Fahoum & Al-Fraihat, 2014).

A wavelet is a short waveform used in signal processing, due to their ability to capture localized events or features in a signal, which provides more information at different scales. There are several types of wavelets, being Morlet wavelet one of them (Cohen, 2014).

The general expression for a wavelet is:

$$\psi_{a,b}(t) = \frac{1}{\sqrt{a}}\psi(\frac{t-b}{a})$$

Equation 3: *Wavelet function.*

In **Equation 3** a is a positive number that defines the scale (dilation), b a real number that states the shift (translation), and *t* means time.

Wavelet transform is used for non-stationary signals (signals in which its statistical properties change over time), as EEG data, to extract time-frequency from raw data. The WT allows variable-size windows, which provides a more flexible way of representing the signal in terms of time-frequency (Al-Fahoum & Al-Fraihat, 2014).

When performing continuous wavelet transform, a time-scale map is created using a wavelet's dilation and translation. A single scale spans a frequency range and has an inverse relationship to the dilated wavelet's time support (Sinha et al., 2005). The scale parameter grants the control of the width of the wavelet in the time domain, which affects the frequency content of analysis. Big scale parameters capture low frequency components, whereas smaller scale parameters capture higher frequency components.

CWT can be expressed as:

$$CWT\ (a,b) = \int_{-\infty}^{\infty} x(t)\Psi^*_{a,b}(t)dt$$

Equation 4*: Continuous wavelet transform.*

In **Equation 4** $x(t)$ represents the EEG signal, a is the dilation, b is the translation factor and $\Psi^*_{a,b}(t)$ stands for the complex conjugate of the wavelet. The continuous wavelet transform is illustrated in **Figure 2.17**.

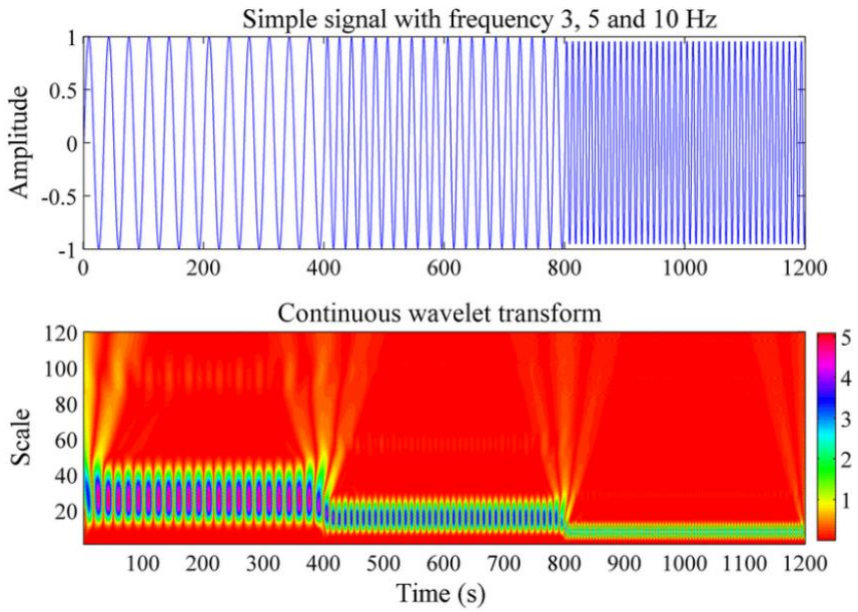

***Figure 2.17**: Illustration of continuous wavelet transform. Adapted from* (Singh et al., 2018).

Between the advantages of CWT, it is worth noting: the freedom that it provides in selecting wavelets to use, the facility to interpret results and the liberty to have any type of time-frequency resolution (Aguiar-Conraria & Soares, 2014; Sinha et al., 2005). However, it requires more computational time than other methods.

When doing wavelet convolution, there is a common artifact associated: edge artifact. Near the signal edges, there are no neighbour points, which makes the convolution incomplete. This turns the signal noisy at the edges (Wu, 2019).

3. Literature Review

3.1. Introduction

Neuroforecasting is a scientific field in which brain activity of a small group is used to predict the behaviour of a separate and independent group. Consequently, a group behaviour can only be predicted in the future (Ancora et al., 2022; Knutson & Genevsky, 2018).

This is a scientific topic with many controversies. In line with this, there are numerous factors that can hide the influence of neural activity and data at the aggregation selection level, such as: unusual individual preferences and random noise. In this way, neuroforecasting should be seen as a tool to complement the behavioural predictions of a group future choice (Ancora et al., 2022; Genevsky et al., 2017).

Neuroforecasting has been used in different areas. For instance, researchers have already targeted the NAc activity to predict album sales containing an examined song (Berns & Moore, 2012), mPFC to forecast call volume in regards to health-related advertisements (Falk et al., 2011). However, its use in the area of urbanism is practically rare.

Neurourbanism is a relatively new field of science in which mental wellbeing is studied together with urban environment (Adli et al., 2017). Also, association of mental disorders with the urban space are studied through neuroscience methods. One of the goals is to prevent mental illness from people who live in cities and promote their well-being (Pykett et al., 2020).

3.2. Methods

In the following section neuroforecasting relevant studies and the most recent advances of this area applied to neurourbanism will be discussed. The articles are displayed in chronological order. The studies were chosen from a set provided by Dr. Diego Andrés Blanco-Mora, based on the relevance for this present dissertation.

3.3. Studies

3.3.1. Berns, G. S., & Moore, S. E. (2012). A neural predictor of cultural popularity.

3.3.1.1. Objectives

In this study (Berns & Moore, 2012) the main goal was to use fMRI to forecast music popularity. To achieve it, they used fMRI while the participants were listening the music from unknown artists. The ultimate goal was to predict the music sales, quoting: “do neural responses to music in an fMRI study predict subsequent commercial success of the song and artist?”.

(Berns & Moore, 2012) state that neuroeconomics showed that the brain regions of reward are predictive of future purchases of the respective individuals scanned. For this to be useful in marketing, it would be necessary to generalize to a larger group of individuals, because it is unknown if the neural activity of a small group is predictive of a large group.

3.3.1.2. Participants

A total of 32 teenagers were recruited for this study, of which 5 participants were excluded due to excessive movement or susceptibility artifacts. Thus, 14 females and 13 males, ages 12 to 17, with a mean of 14.6 years, were present.

Before the experiment, the participants were screened for the presence of psychiatric diagnoses.

3.3.1.3. Methodology

Auditory stimuli were applied using songs of unknown artists with a duration of 15 seconds per clip. The set of clips was selected from each participant's top three genres, using 20 clip songs per music genre. A study session contained 60 trials, with each trial divided in two stages. In the first stage, the subject listened to the music and rated the song based on how familiar it was and their likeability. The second stage consisted on listening the same music so that the participant could rate the song again, according their likeability. In 40 trials the song's popularity was shown during the second stage. The study paradigm is presented in **Figure 3.1**.

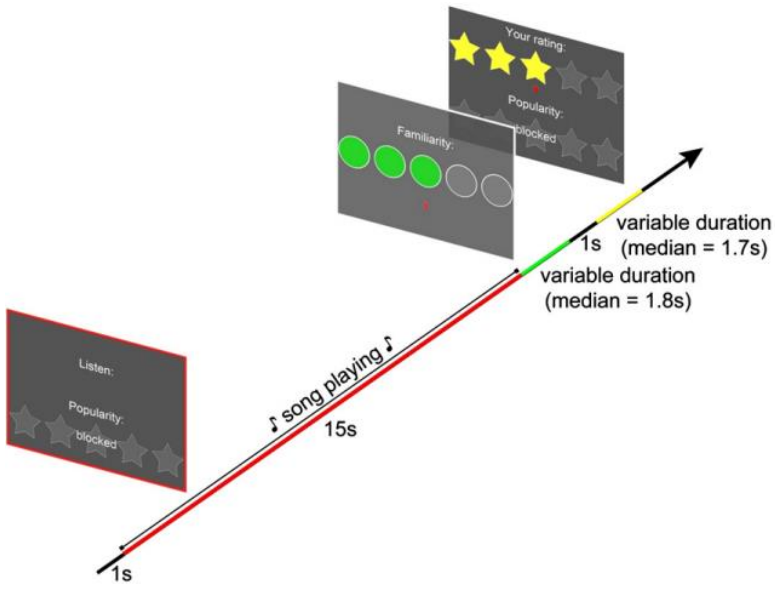

***Figure 3.1**: Study design. First, the participant listened to the music for 15-s (red). Then, the participants were required to rate the level of familiarity (green) and likability (yellow). Retrieved from (Berns & Moore, 2012).*

3.3.1.4. Results

The results of this study showed that there were three brain areas that had a correlation between the activation and the song likability: nucleus accumbens, orbitofrontal cortex and cuneus. According to the reported results, only three of the songs were commercially successful, which means that the subjective rates from the participants might not be a reliable predictor of commercial success.

However, (Berns & Moore, 2012) found that the NAc activity is significantly correlated with the commercial success, as illustrated in **Figure 3.2**. These results evidence that brain responses to products not only predict purchasing decisions of actually scanned individuals, but that also such responses can be generalized to entire populations and used to forecast cultural popularity.

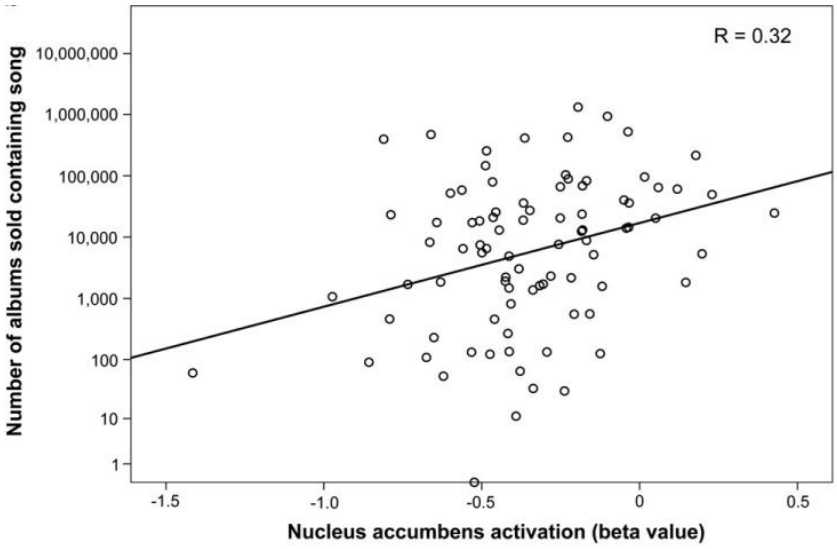

***Figure 3.2**: Correlation between the log of song sales and the average nucleus accumbens activation during song listening. Retrieved from (Berns & Moore, 2012).*

3.3.2. Dmochowski, J. P., Bezdek, M. A., Abelson, B. P., Johnson, J. S., Schumacher, E. H., & Parra, L. C. (2014). Audience preferences are predicted by temporal reliability of neural processing.

3.3.2.1. Objectives

(Dmochowski et al., 2014) designed a study to record the brain activity from a group of people while they were watching popular television content. The main question of this study is "whether the neural activity of multiple individuals may collectively predict the behaviour of large groups".

Since the television content has already aired when the study started, (Dmochowski et al., 2014) collected aggregate measures of the population feedback.

3.3.2.2. Participants

There were 41 contestants in all. The participants were divided into three groups for the experiment: 'The Walking Dead' pilot episode was watched by 16 healthy subjects (nine females and seven males, ages 19 to 32, mean of 26 years); 10 advertisements were viewed and rated by 12 subjects (gender balanced, ages 20 to 29; mean of 25 years); and the same batch of *Super Bowl* commercials from 2012 and 2013 were seen by 14 subjects (six females, ages 18 to 22, mean of 20 years).

3.3.2.3. Methodology

The neuroimaging techniques used were fMRI and EEG. EEG was utilized in the first two studies to capture neural activity while the participants watched television, and fMRI was employed in the third experiment. The first experiment consisted of assisting one episode of the TV series *The Walking Dead*. The episode was divided in 190 scenes. For each scene the frequency of elicited tweets (obtained through a list of all episode-related tweets that were posted between 9:00-10:00 PM October 31st 2010, containing a relevant hashtag, a mention of a show-specific Twitter account or merely mentioned the show's name) was computed. The degree of inter-individual correlation in evoked EEG responses was found to predict expressions of interest and preference in thousands of people.

(Dmochowski et al., 2014) wanted to test the reliability of neural sampling for its ability to predict preferences for different stimuli. Thus, for the experiment 2, 12 subjects were recruited to watch 10 commercials from *SuperBowl* 2012 and 10 adds from *SuperBowl* 2013, while also recording EEG. With this, a significant correlation between the population ratings and the neural reliability was found.

In the third experiment, a fMRI experiment was performed using 14 participants in which was recorded the BOLD signal from the 10 ads.

3.3.2.4. Results

As for the first experiment, the sample's neural reliability during each scene accounts for 16% of the variation in audience log tweet frequency, as seen in **Figure 3.3**.

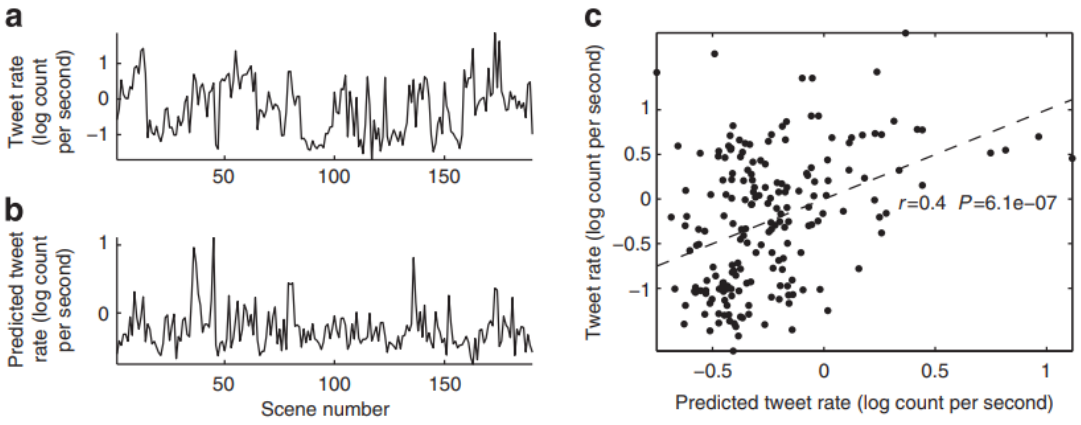

***Figure 3.3**: Scene-by-scene tweet frequency is predicted using neural reliability. (a) The number of times each scene from a popular television show was mentioned on Twitter. (b) Log tweet frequency predicted from scene-by-scene neural reliability measured across 16 participants. (c) The log tweet rate's variance is 16% explained by neural reliability. Retrieved from* (Dmochowski et al., 2014).

The second experiment showed that neural reliability accounts for 66% of the variation in population assessments, as shown in **Figure 3.4**.

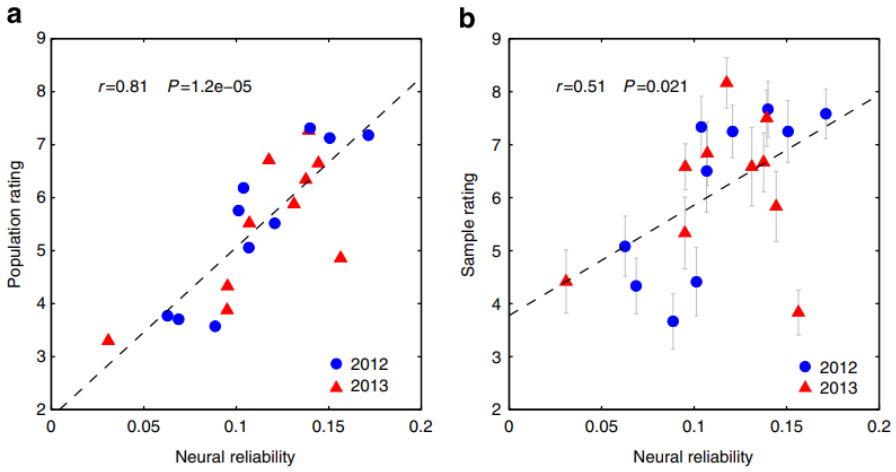

***Figure 3.4**: Neural reliability in small samples predicts preference ratings for large numbers of viewers. (a) Dashed lines show linear predictions of population ratings from neural confidence. 66% of the variance in population ratings is explained. (b) Only 26% of sample rating variance is explained. Retrieved from* (Dmochowski et al., 2014).

Regarding the third experiment, (Dmochowski et al., 2014) discovered a significant covariation of the BOLD signal with the EEG neural reliability in both lateral temporal cortices, as represented in **Figure 3.5**.

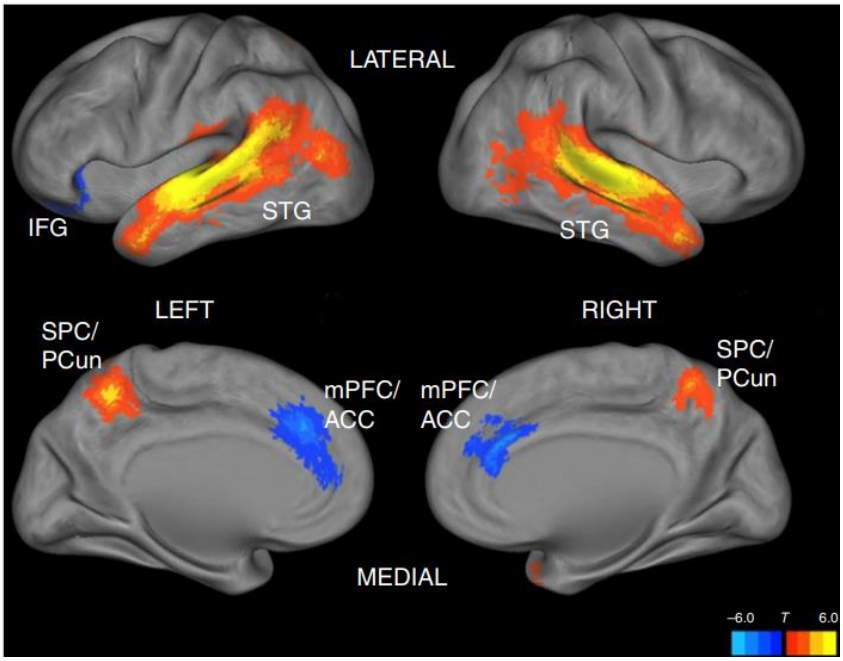

***Figure 3.5**: Neural reliability of EEG-derived and covariation of BOLD signals in different brain regions. The activation clusters visible are: inferior frontal gyrus (IFG), superior temporal gyrus (STG), superior parietal cortex/precuneus (SPC/PCun) and medial prefrontal cortex/anterior cingulate cortex (mPFC/ACC). Retrieved from* (Dmochowski et al., 2014).

With this experiment, (Dmochowski et al., 2014) concluded that measures of behavioural responses aggregated across a large audience were significantly correlated with neural reliability evoked by appropriate naturalistic stimuli in small groups.

3.3.3. Zhu, X., Gao, M., Zhang, R., & Zhang, B. (2021). Quantifying emotional differences in urban green spaces extracted from photos on social networking sites: A study of 34 parks in three cities in northern China.

In conformity with (Zhu et al., 2021) the fast growth of population in cities and, consequently, a fast urbanization has led to some mental disorders, such as anxiety and life pressure. One of the possible solutions might be adding more green spaces to cities, as pointed by (Shekhar & Aryal, 2019). This can be easily understood when thinking about the COVID-19 pandemic period. People felt more negative feelings, especially those who quarantined and they needed to leave their houses and spent some time in green and natures spaces.

3.3.3.1. Objectives

The aim of this study was to pull out the emotions from pictures with geographic information tags on Sina Weibo – a popular social media in China – and to quantify the same emotions at urban green spaces. Thus, the main questions of the experiment are, quoted:

- "Research question 1 (RQ1): Are there differences in the probability of emotions between genders and among ages in urban green spaces?"

- “Research question 2 (RQ2): Are the characteristics of urban green spaces, such as their sizes, normalised vegetation index (NDVI), transportation characters, and types, related to the reported emotions within?”
- “Research question 3 (RQ3): Do the cities present any differences in the emotions in urban green spaces?”

3.3.3.2. Methodology

To perform the study, 34 parks in the following cities were selected: Harbin, Changchun, and Shenyang. Then, Python was used to examine all geographically designated pictures taken within urban green spaces. The emotional indicators used were: emotion probability index (0-100), emotion intensity index (0-1), and emotion evenness index (0-1).

3.3.3.3. Results

The results suggest more intense emotions on women than on men, as shown in **Figure 3.6**, this being the answer for research question number one.

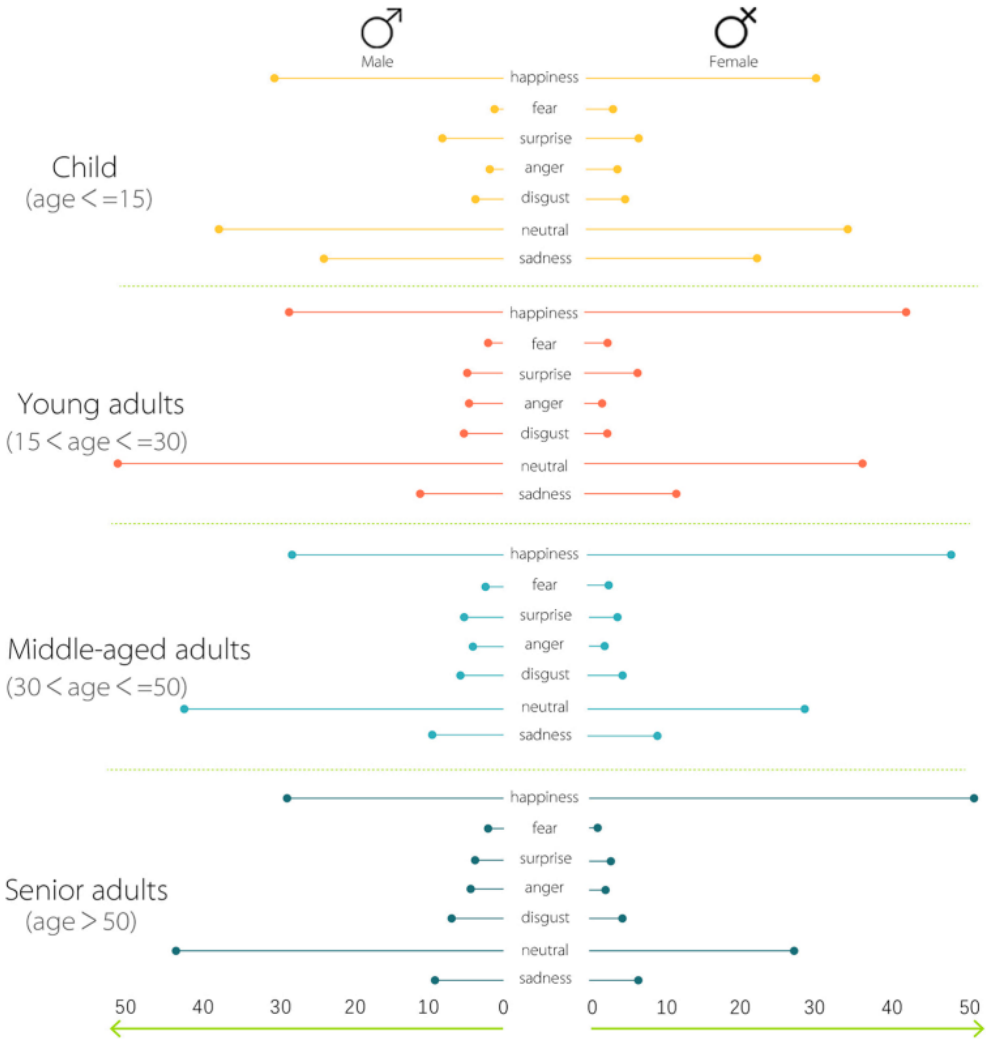

***Figure 3.6**: Emotional differences between male and female genders in different age groups. Retrieved from* (Zhu et al., 2021).

Regarding the research question number two, the results showed a significant positive correlation between happiness and area (green or urban environments) and a negative correlation between space and anger, distance, fear and happiness. Besides this, there is no significant correlation between public transit and the seven basic emotions.

Concerning the research question number three, (Zhu et al., 2021) found out that the three cities have quite identical patterns about the emotions triggered by urban green spaces, as visible in **Figure 3.7**.

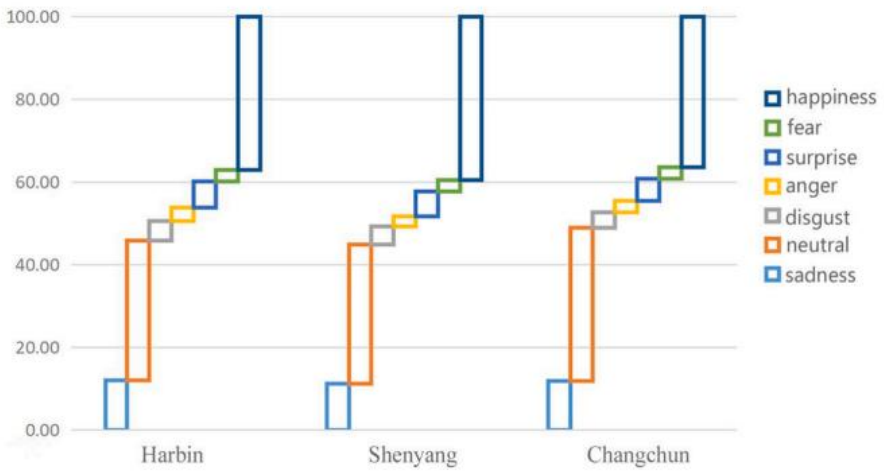

Figure 3.7: *Emotion differences in the three cities. Retrieved from* (Zhu et al., 2021).

3.3.4. Mavros, P., J Wälti, M., Nazemi, M., Ong, C. H., & Hölscher, C. (2022). A mobile EEG study on the psychophysiological effects of walking and crowding in indoor and outdoor urban environments.

According to (Mavros et al., 2022) , it is expected that by 2050 around of 60% of the world population is living in cities. It is also known that the urban environment shapes the way people feel and their mental health. Thus, it is important to know how the crowded environments in the city affect and will affect people's life.

In compliance with Attention-Restoration Theory (ART), urban environments are followed by high levels of stimulation of all human senses. Conversely, green environments require human attention in a different way, reduce stress and enhance cognitive function. Besides this, ART states that being exposed to green environments reduce psychological and physiological stress, leading to positive affect.

3.3.4.1. Objectives

The goal of this study was to compare the experience of walking indoor versus outdoor with a nature baseline, in order to study psychological responses of the different urban environments.

3.3.4.2. Participants

For the experiment, 42 participants were recruited, of which 20 were female and 22 were male. The age range was 19-32 years-old, with a mean of 22.3.

3.3.4.3. Methodology

Self-reported measures combined with EEG and electrodermal activity (EDA) were obtained from the participants. Six videos of walking on a sidewalk in a city were the stimuli set, while walking or standing on a treadmill. The setup and procedure are represented in **Figure 3.8**.

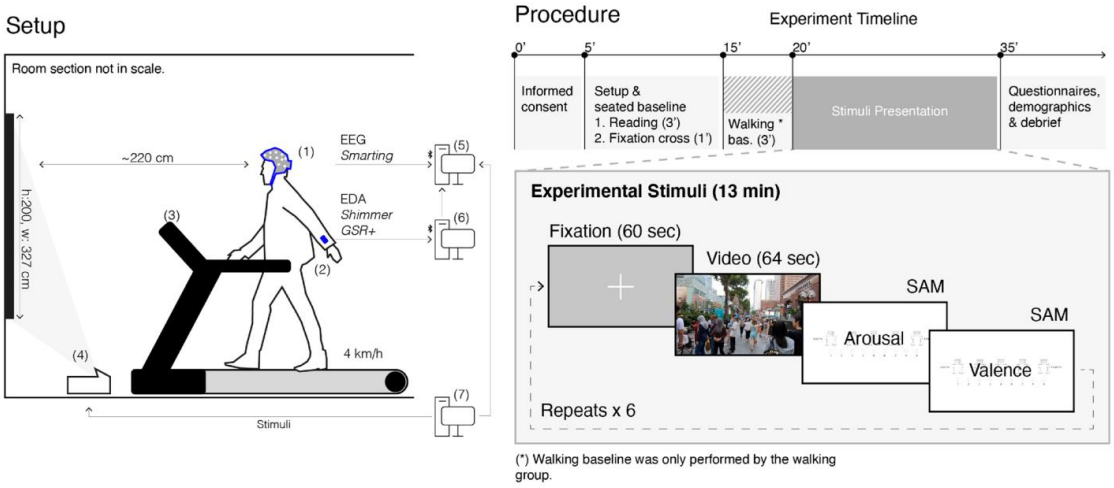

***Figure 3.8**: (Left) Experiment setup, in which the participants has to walk or stand while watching videos. (Right) Experiment timeline with the respective paradigm. Retrieved from* (Mavros et al., 2022).

3.3.4.4. Results

The results reported by the subjects showed more positive emotions and lower arousal after watching nature videos, compared to the urban environments. In addition, the initial hypothesis that crowded scenes evoke lower valence and higher arousal in the subjects was confirmed.

3.4. Discussion

The four studies analysed showed important findings. The first two (Berns & Moore, 2012; Dmochowski et al., 2014) are related to neuroforecasting, whereas the last two studies (Mavros et al., 2022; Zhu et al., 2021) are applied to the field of neurourbanism.

In the first study, (Berns & Moore, 2012) showed that while likability of the songs was not predictive of future sales, the brain activity in ventral striatum was significantly correlated to the units sold. These results evidence that brain responses can be generalized to a large group of population and be predictive of cultural popularity.

In the second study, (Dmochowski et al., 2014) evidenced that the inter-subject correlation evoked responses in the electroencephalogram are predictive of preference and interest among thousands of people, when watching popular broadcast content. This suggests that the pleasurable stimuli for a person might be those for which the brain responds in a stereotypical way shared by other people.

The third study, (Zhu et al., 2021) showed that, based on three emotion-based indexes, there are some significant correlations between variables like: age, gender, emotion, accessibility, area and emotional diversity. The results also evidence that green space planning can be used to mediate the people's emotions. With this, it is concluded that improving the cities green space can be a great mechanism to stabilise the human emotions.

Finally, in the fourth study, (Mavros et al., 2022) evidenced that green spaces are perceived as more calm and positive spaces, by measuring the EEG and EDA responses to walking or standing in different urban environments. Besides this, crowded scenes induced higher self-reported arousal and negative valence and required more cognitive resources. This study suggested that it is possible to use EEG and EDA in an ambulatory scenario.

***Table 2**: Studies summary.*

Title	Neuroimage Method	Experiment	Findings
A neural predictor of cultural popularity.	fMRI.	Measuring brain responses in a small group of teenagers, while listening to unknown artists.	Brain responses can be generalized to a large group of population and be predictive of cultural popularity.
Audience preferences are predicted by temporal reliability of neural processing.	fMRI and EEG.	Recording brain activity from a group of individuals while watching a popular TV show and commercials.	The degree of inter-subject correlation in evoked brain responses predicts expression of interests and preferences by thousands.
Quantifying emotional differences in urban green spaces extracted from photos on social networking sites: A study of 34 parks in three cities in northern China.	Python.	Examining all geographically designated pictures taken within urban green spaces.	There are some significant correlations between variables like: age, gender, emotion, accessibility, area and emotional diversity. Also, green space planning can be used to mediate the people's emotions.
A mobile EEG study on the psychophysiological effects of walking and crowding in indoor and outdoor	EEG and EDA.	Six videos of walking on a sidewalk in a city were the stimuli set, while walking or standing on a treadmill.	Green spaces are more calm and positive spaces, and crowded spaces evoke a higher

urban environments.			arousal and negative valence.

3.5. Conclusion

Neuroforecasting applied to urbanism is an emergent field that can be used to prevent mental disorders and promote the well-being of people in big cities (Fett et al., 2019).

Despite growing evidences of the impact of green spaces in an urban environment, more studies are still needed to see how the cities' design in the future can be a useful tool, since neurourbanism is a relatively new field of science. Also, it is important to delve deeper into the issue of using brain activity as predictor of other variables, because it is something barely done in neurourbanism.

4. Materials and Methods

4.1. Description of the Study

The Brain as Predictor (BAP) experiment is part of the eMOTIONAL Cities project. This project is co-coordinated by Instituto de Geografia e Ordenamento do Território (IGOT) and by Faculdade de Medicina da Universidade de Lisboa (FMUL). The experiment includes several international partners. The goal of eMOTIONAL Cities is to provide evidences about how urban environment shapes the human being emotional and cognitive processing.

I contributed to this study in two ways: on the one hand, I helped with the practical part, namely in preparing the setup and helping with other aspects during the experiment. On the other hand, I helped with data analysis, trying to explore new ways of analysing it.

4.2. Objectives of the Study

BAP experiment uses simultaneous EEG and fMRI to study the human brain activity, with the aim of evaluating the potential of using brain activity as a predictor for evaluating the impact of urban spaces on human beings.

4.3. Research Questions

The next sections of this thesis will delve into the two major issues that have guided the research. First, the goal is to determine whether EEG signal analysis can assist in comprehending how much people enjoy various locations and how the human brain respond to them. Then, using images of locals versus visitors, it will be performed image analysis to determine if there is anything unique about the EEG signals. To sum up:

1. Can spectrum analysis of EEG signals be used to accurately represent the popularity of environments? If so, how is the relation between brain activity and popularity of environments described?
2. Is there any significant difference in the spectrum analysis of EEG signals between the two groups of images (resident and tourist)?

In this way, my work aims to expand the literature review by using ERS/ERD to see if it can work as a predictor of popularity of images. Whereas some studies used brain activity to predict cultural popularity (Berns & Moore, 2012; Dmochowski et al., 2014), this dissertation will use ERS/ERD to analyse the possibility of being a predictor of not cultural popularity, but popularity of an urban image. Basically, it is the combination of (Berns & Moore, 2012; Dmochowski et al., 2014) with the second research question of (Mavros et al., 2022).

Understanding if brain activity can be used as a predictor of an image's feature (popularity in this case) is something never done in the literature review and that can be a good starting point to promiscuous studies in neurourbanism area.

Besides this, analysing the differences in brain activity between pictures taken by residents and by tourists is something new to the neurourbanism field. Typically, we think that touristic pictures will be associated to touristic areas in the cities and that will cause more pleasure to the person who is watching, whereas the resident pictures will be associated to resident spots, such as houses and urbanizations, which will not cause so much pleasure, in theory. That is why it will be interesting to see if the differences between the two groups are significant and accordingly to what is expected.

4.4. Study Design

4.4.1. Paradigm

The goal of the Brain as Predictor experiment was to determine whether or not brain activity could be used as a predictor to assess how urban environments affect people, being the experiment paradigm based on (Berns & Moore, 2012). A set of pictures from Lisbon with different urban environments were used as visual stimuli in healthy subjects. The participants rated each image following the paradigm described in **Figure 4.1**.

The beginning of each trial contains a blank screen for a variable period between 0 and 1 second. After it, a black cross appears in the centre of the screen and lasts between 2 and 3 seconds, following a Poisson distribution (a total of 4 seconds for these two blocks). Then, a photo from the dataset is presented and the subject must rate it in a maximum of 4 seconds with a provided joystick on a scale of 1 to 4. After rating, a number of highlighted stars corresponding to the scoring mark will appear on the screen (a total of 4 seconds for these two blocks). The order of image appearing is random and without repetition. This means that the total duration of each block is 8 seconds. Participants went through two sessions comprehended of 80 images each, where the total duration of each task is 640 seconds. Next, after a brief break for the participant, the second session is started. The total duration of the data acquisition is 1280 seconds.

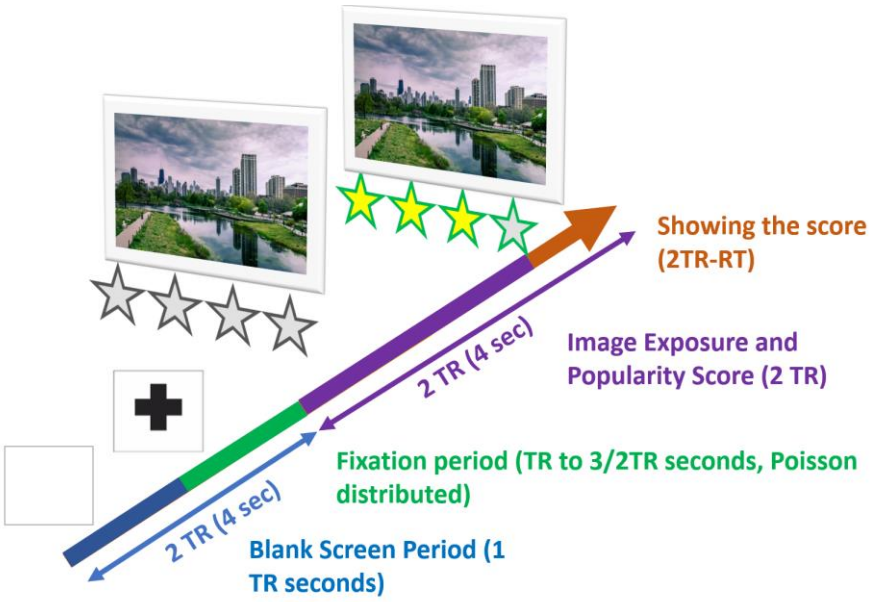

***Figure 4.1**: BAP experiment design.*

4.4.2. Set of Images

Flickr, an image and video hosting service, provided a set of 160 images from the Lisbon area. According to the status of the photographer (residents vs tourists), images were divided into two possible groups. If a photographer's Flickr account posted photos from Lisbon inside the specified geographic parameters for more than three months in a row, they were given the presumed resident classification.

There are 80 images in each of the two groups, Resident and Tourist. Each image has the following info: green index, calculated using the normalized difference vegetation index (NDVI); cell density, which is the number of photos per 100 meters (cell) of the city that are from the same city area; number of views, which is the total number of views on Flickr; and popularity index, which normalizes the number of views against the photographer's highest number of views.

4.4.3. Participants

4.4.3.1. Participants Demographics

A total of twenty-five healthy participants with ages between 18 and 35 years ($mean = 23.1$ and $std = 3.24$) were recruited. In terms of gender, there were 13 males and 12 females. All this information is represented in **Figure 4.2**. Participants were recruited via in-person recruitment on the university campus.

According to (Cohen, 2014), for cognitive studies at least 20 participants must be recruited so that it is possible to identify large and subtle effects and to conduct assessments of individual differences and correlation.

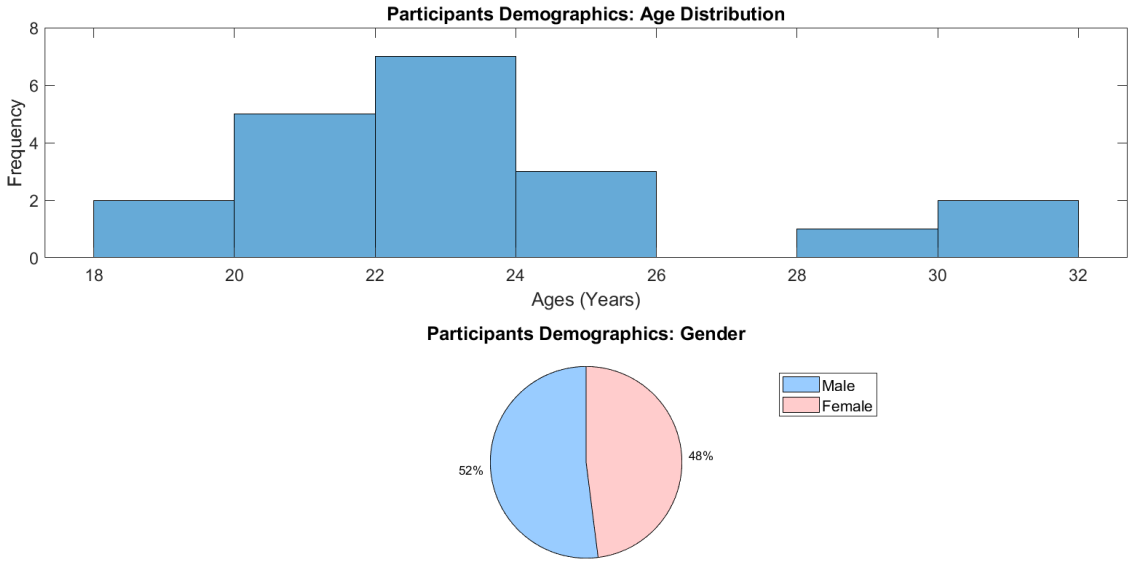

***Figure 4.2**: Participants demographics summary. (Upper graphic) Histogram with participants' age distribution. (Lower graphic) Pie chart with the gender distribution.*

4.4.3.2. Inclusion and Exclusion Criteria

Inclusion criteria for subjects to be selected were: age between 18 and 35 years old and clear vision (or even corrected with contact lenses).

To carry out the experiment, participants must fulfil a questionnaire to see if they are suitable, as well as a consent.

The exclusion criteria for BAP experiment, meaning, the characteristics of eligible subjects that make them highly likely to develop diseases or cause death after the experiment or provide inaccurate data are: having a pacemaker; osteosynthesis material, plates/screws; coronary stents or artificial heart valves; metal objects or swarf on the body; cochlear implants or metal tubes in the ears; dental appliance/prosthesis or orthodontic material; central venous catheter; infusion pump; transdermal systems; being pregnant, being claustrophobic, history of neurological or psychiatric disorders or cognitive impairment, use of medication affecting central nervous system and epilepsy or history of epileptic seizure. All these exclusion criteria is due to the MRI scanner.

4.4.4. Experimental Procedure

The next subchapter describes the experimental protocol applied to each participant in the lab.

4.4.4.1. Protocol

1. **Informed Consent and Assessments**

   Information was collected from some forms and assessments:

   a) The inclusion and non-inclusion criteria for participation in the experiment. This is mostly because of the ferromagnetic materials that are not allowed inside the MRI, as well as claustrophobia, neurological disorders and other important exclusion criteria;
   b) Informed consent;
   c) DASS-21 (Depression Anxiety and Stress Scale);
   d) PANAS (Positive and Negative Affect Schedule);
   e) BIS/BAS (Behavioural Inhibition System/Behavioural Activation System).

2. **EEG Cap Preparation**

   a) First, the head perimeter of the subject is measured to find out which EEG cap is more suitable;
   b) Then, the nasion-inion and LP-RP distances are measured to find the Cz (reference) location;
   c) After this, it is time to prepare the saline solution (1 L water, 11 g salt and 5 mL shampoo);
   d) The EEG cap must be in the prepared solution during 10 minutes and then it is ready to be placed in the participant;
   e) An important fact is to ensure the safety of the participants taking care of the EEG wires, which can present loops. The small loops act like coils and receive induced currents

from the MRI magnetic field, heating the electrodes and potentially causing burns to the participant's scalp.

3. ***GeoScan***
   a) When using the *GeoScan*, first it must be turned on and wait for the stereo camera to warm up;
   b) Then, the electrodes were scanned (up to 2% of the electrodes on the EEG cap can be left out of the scan);
   c) Finally, the EEG reference markers were scanned with the probe.

4. **Checking the Impedances**
   a) First of all, the electrodes impedance must be checked to see if it is between 0 and 10 kΩm;
   b) When necessary, more saline solution was added on the electrodes with worse impedance, having in mind to avoid adding too much solution. Otherwise, there will be a short circuit and the neighbouring electrodes will transmit the same signal.

5. **ECG Placement and Participant Accommodation inside the MRI**
   This part is done by the MRI technician.

6. **fMRI-EEG Preparation**
   In this part of the study, the distinct parts of the experiment were explained to the participants.

7. **Resting State**
   a) First, the subject was informed to be in a resting state while looking to the cross (5 minutes);
   b) Then, the participant was asked to close their eyes and try to imagine the cross (5 minutes).

8. **Training Task**
   To get familiar with the joysticks, the subject was requested to perform a training task.

9. **Task 1**
   The participant was asked to score 80 images (shown randomly for all participants) with the joysticks (11 minutes).

10. **Task 2**
    The subject was requested to score 80 images (shown randomly for all participants) with the joysticks (11 minutes).

11. **Final assessments**
    The last thing the subject was asked was to fill three final assessments: Bergen, Hexaco and Satisfaction with Life Scale.

12. **EEG Cap Cleaning**
    a) First, the cleaning solution was prepared (2 L of water and 20 mL of sanitizer);

b) Then, EEG cap was dipped and raised on a bowl with the solution during 2 minutes;
c) After this process, the EEG cap was left inside the solution bowl during 8 minutes;
d) Then, the cleaning solution was poured and the bowl was filled only with water;
e) Finally, the EEG cap was sank and lifted up on the water bowl 4x20 times.

4.4.4.2. Timeline

When the participant is ready for getting in the MRI, the resting state and the two tasks should take no longer than 40 minutes. In total, the experiment takes around two hours. **Figure 4.3** represents a timeline for the experimental procedure.

***Figure 4.3**: Representation of the experimental procedure timeline.*

4.4.5. Hardware and Software

4.4.5.1. EEG

The EEG set is composed by the EEG amplifier and the EEG cap. The EEG used for the experiment was a GES 400 MR (*Geodesic EEG System 400 Series*, 2021), which is a HD-EEG of 257 channels, with Cz as reference, and an extra electrode COM as electrical reference/ground. This EEG set has a special and important feature: compatibility with MRI (*EEG Systems Compatible with MR and MEG Environments*, 2021).

Besides this, to capture and amplify ECG data, the EEG amplifier works as a Faraday cage to reduce MRI ambient noise. The EEG amplifier is powered by a power supply, which works as a voltage regulator to maintain a steady power supply.

The EEG cap is a product of *Magtism EGI* and there are 3 sizes available: small (54 cm – 56 cm), medium (56 cm – 58 cm) and large (58 cm – 61 cm). The measures in centimetres are for the subjects' head perimeter. The EEG cap electrodes are passive and wet.

Figure 4.4 shows of one of the three EEG caps used.

***Figure 4.4**: EEG cap used for the experiment. Developed by Magtism EGI.*

4.4.5.2. MRI

A Siemens 3T magnet was employed for the experiment described in section 4.4. This dataset had a spatial resolution of around 6 mm^3 (1.41 x 1.41 x 3 mm (voxel volume)). To acquire the MRI images (structural and functional), the RM Philips Ingenia scanner was used.

The stimulus computer displays stimuli on the MRI room screen through Psychtoolbox (Pelli & Vision, 1997) in MATLAB (Matlab, 2012) to perform the experiment protocol.

4.4.5.3. Software

For this experiment, five different softwares for data acquisition and analyses were employed:

1. *Net Station Acquisition* (*Net Station Acquisition for Routine EEG Data Collection: Video Tutorial*, 2021), developed by *Magtism EGI*: to record the EEG data.
2. *GeoScan* (*GeoScan Handheld Sensor Digitization*, 2021), developed by *Magtism EGI*: to scan all the EEG electrodes. The EEG electrodes are scanned using reflexion principles, through a stereo camera.
3. *Psychtoolbox* (Pelli & Vision, 1997) used for stimuli presentation, following the previously described paradigm in 4.4.1.
4. *MATLAB* (Matlab, 2012): to run the experiment with *Psychtoolbox* (Pelli & Vision, 1997) and to read the serial signals from the joysticks.
5. *R* (Matloff, 2011): to perform statistical analysis with the EEG data.

4.4.5.4. Communication Between Devices

There are various devices in the experimental setup that allows the communication between the core equipment.

Communication between the acquisition computer and EEG amplifier is made possible by a router.

The EEG Acquisition computer scans electrodes with *GeoScan* (*GeoScan Handheld Sensor Digitization*, 2021) and archives EEG data using programs like *Net Station Acquisition* (*Net Station Acquisition for Routine EEG Data Collection: Video Tutorial*, 2021). *Psychtoolbox* (Pelli & Vision, 1997) was used in *MATLAB* (Matlab, 2012) to carry out the experiment protocol, the Stimulus computer displays stimuli on an MRI room screen using HDMI. Participants can rate the images using joysticks, from *NordicNeuroLab* (*FMRI Acquisition | NordicNeuroLab*, 2023).

The Syncbox (*FMRI Acquisition | NordicNeuroLab*, 2023) gets the MRI triggers from the MRI scanner and joysticks responses.

Together, these components synchronize data, record participant reactions, capture and interpret EEG/ECG signals, and manage stimulus presentation throughout the experiment.

The MRI is connected to the EEG-MR Clock Synchronizer (the Net Amps Clock Sync) and the Syncbox using a coaxial cable communicating the MRI trigger at each volume acquisition and joysticks response. The Net Amps Clock Sync synchronizes the EEG and MRI scanner clocks, and sends the MRI trigger signal to the EEG amplifier. The syncbox communicates the MR trigger signal and the joysticks response to the stimulus computer via serial communication (USB). The stimulus computer communicates the time stamps (events, e.g. blank, cross, image exposure), to the EEG amplifier using TCP/IP protocol.

The EEG amplifier transmits the EEG data, time stamps, and stimulus to the acquisition computer.

5. Data Analysis

Data analysis was performed with MATLAB 2018 (Matlab, 2012) and R (Matloff, 2011) was used for statistical analysis.

The present work is focused on EEG. Therefore, the data from fMRI will not be used. fMRI was mentioned, because the BAP study used EEG-fMRI combined.

5.1. Pre-Processing

Pre-processing is one of the most important steps, after getting the EEG signals. EEG raw data can be sometimes very noisy and difficult to analyse. Consequently, it is important to clean the EEG data (Suárez-Revelo et al., 2018), by removing artifacts present in the signal, in order to increase the signal-to-noise ratio (SNR) – a ratio of recording's signal to noise power (Johnson, 2006). Rejecting extraneous influences while maintaining the neuronal response will increase signal quality.

The next sub-chapters will describe the steps performed in order to clean the EEG data. The cleaning scripts were developed by Dr. Diego Andrés Blanco-Mora by using Eeglab (Delorme & Makeig, 2004) functions.

5.1.1. EEG Software and Artifacts Removal

To perform the initial pre-processing, EGI offered a software with a specific set of tools that made it faster than MATLAB-based algorithms to input data, remove BCG (ballistocardiogram) artifact, and gradient removal. In the EGI software, the average window method with N=35 (number of averaged triggers) to eliminate the gradient artifact was used. The OBS (optimal basis steps) method – choosing the best basis functions or representations to use while analysing and processing a particular signal – was used to remove BCG after BCG peak identification using the qrs complicated detection module. Following the standard pre-processing stages, the EEG data is processed once MRI-induced artifacts have been eliminated. As a result, Eeglab (Delorme & Makeig, 2004) was used in MATLAB to carry out the operation.

5.1.2. Slicing Effect

After using EGI software to clean the gradient effect, there was a remaining slicing effect, still present in EEG data. Basically, in the power spectra density representation, some spikes are visible at constant frequencies. These frequencies are given by:

$$f_{slice} = \frac{slices\ number + 1}{TR}$$

***Equation 5**: Slicing effect.*

As the slices number in our experiment is 35 and TR is 2, the result will be 18 Hz, because the number of triggers in a second are 36. This effect can be present at the main frequency (18 Hz in this case) and in its harmonics (36 Hz, 54 Hz, 72 Hz, etc). However, the pulse representation is not ideal, and it can occupy neighbourhood frequencies. In this way, the spikes are visible in this frequency harmonics (18, 36, 54, etc). **Figure 5.1** represents the effect described.

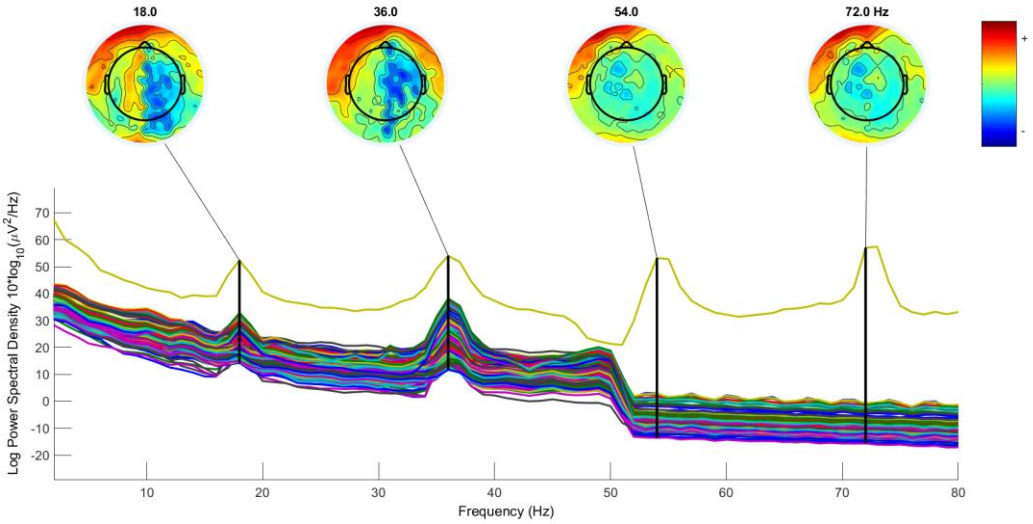

Figure 5.1*: Slicing effect. It is visible spikes in the log power spectral density at these frequencies: 18 Hz, 36 Hz, 54 Hz, 72 Hz. Around the 52 Hz frequency, the data was filtered with EGI software, which changes the log power spectral density.*

5.1.3. Remove Channels and Filtering

First, the ECG channel was discarded, since its only purpose was to remove the BCG artifact. Once the BCG artifact was already removed in this process stage, then the ECG channel is useless for the EEG spectral analysis. To do that, the *pop_select* (Delorme & Makeig, 2004) function was used.

After this, the data needed to be downsampled. In order to reduce the computational time, increase SNR, and avoid redundant frequency information (Muhammad et al., 2020), downsampling should be performed. The acquisition sample rate was 1 kHz, then EEG data was downsampled by a factor of 8, which makes a 125 Hz sample rate, using *pop_resample* (Delorme & Makeig, 2004) function. The donwsampling process is essential to a more efficient and accurate analysis of the EEG signals.

Then, a bandpass filter with *pop_eegfilt* (Delorme & Makeig, 2004) function was applied on the data to limit the frequency information. The low edge frequency was 0.5 Hz and the high edge frequency was 32 Hz. First, it is necessary to apply a high pass filter at the cut off frequency of 0.5 Hz so that the Independent Component Analysis (described further ahead) (ICA) solution is more stable (Rodrigues et al., 2021), because there is no low frequency present. Second, the low pass filter at the cut off frequency of 32 Hz is applied, because the signals of interest are under 32 Hz, meaning the EEG rhythms. Thus, by excluding the signals above 32 Hz, the computational complexity is reduced. Processing and analysing high-frequency signals often require a higher computational power. Therefore, by eliminating these high-frequency signals, the dataset becomes less heavy and the computational performance becomes finer.

5.1.4. Aggressive Cleaning

After all the cleaning described, it is time to remove bad channels and bad data portions. Therefore, the *pop_clean_rawdata* (Delorme & Makeig, 2004) function is used. For this, a channel is removed under the following criteria: the channel is flat (zero-value) for more than five seconds – *FlatlineCriterion*; the channel has a high amount of noise, based on a standard deviation value higher than 4; and the channel is low correlated with other channels, with a value lower than 0.8 (Delorme & Makeig, 2004).

When *FlatlineCriterion* is active, the EEG reference (*Cz* in this case) will be marked as flatted and, consequently, removed. Thus, *Cz* must be recovered back by removing *ref_label* from the deleted channels.

5.1.5. Interpolation

The noisy channels removed must be interpolated. Interpolation is the process of estimating and filling the removed/missing EEG data. For this purpose the *pop_interp* (Delorme & Makeig, 2004) function was used, with spherical interpolation. Spherical interpolation estimates the missing data based on the surrounding EEG electrodes values.

Finally, EEG data was re-referenced. Re-referencing is a crucial step in EEG data pre-processing, whose purpose is to transform the EEG data from a certain reference to a reference relative to a common average. In this case, the average referencing method was used, utilizing *pop_reref* (Delorme & Makeig, 2004) function with all channels as reference.

5.1.6. Independent Component Analysis

To perform the ICA in MATLAB, a function called *ica_criterion* was created which uses the *pop_runica* (Delorme & Makeig, 2004) function to compute ICA.

When running ICA in MATLAB, the software provides the progress of the algorithm, showing three parameters: *lrate*, *wchange* and *angledelta*. The first one is the learning rate, which regulates the algorithm's step size and is typically decreased at each ICA iteration to prevent overshooting the ideal answer (Hyvarinen, 1999). The projected weights' change between the current iteration and the previous one is measured as *wchange*, which shows how quickly the algorithm is converging to the optimal solution (Hyvarinen, 1999). Finally, *angledelta*, a measure of stability, is the difference in angle between the predicted weights in the current and previous iterations (Hyvarinen, 1999).

ica_criterion is based on seven ICA classes: brain, muscle, eye, heart, line noise (when monitoring biological signals like EEG or fMRI, recording equipment may pick up extraneous electrical signals), channel noise and other. To classify each component in each of the last classes, the *pop_iclabel* (Delorme & Makeig, 2004) function is used. As mentioned in section 2.5.1 it is mandatory to have a threshold value to reject those components with a higher value. In this case, these thresholds (in a scale from 0 to 1) were: 0.5 for the eye, 0.7 for the heart, line noise and channel noise.

5.1.7. Clean EEG Signal

After all these pre-processing steps described, the EEG signal has a smoother shape than the original one (**Figure 5.1**), as shown in **Figure 5.2**.

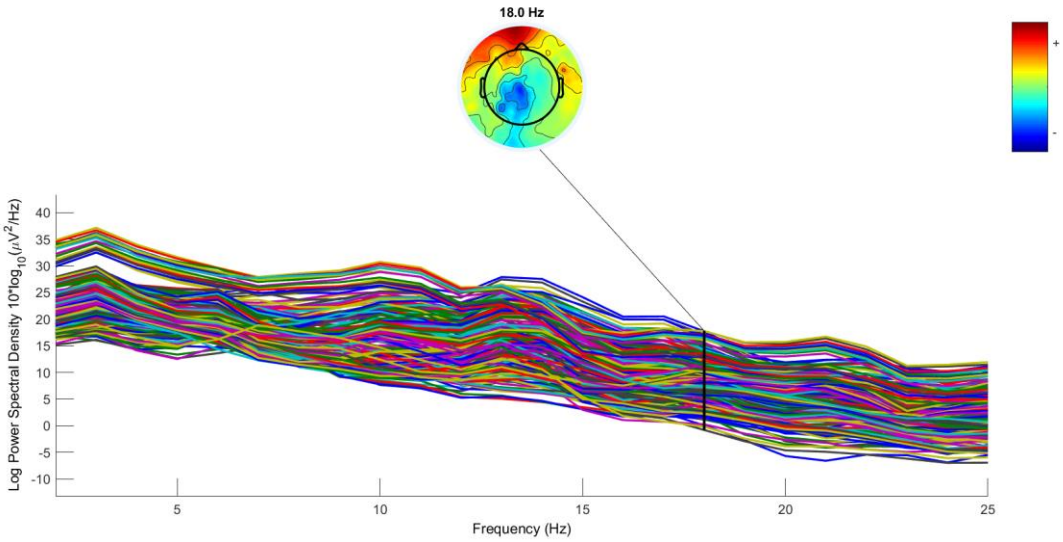

***Figure 5.2**: Power spectral density after all pre-processing.*

5.2. Time-Frequency Analysis

5.2.1. Wavelet Method

Time-frequency representation was obtained through wavelet convolution, between EEG signal and wavelets from different frequencies. This method follows the methodology described in (Van Hoornweder et al., 2022), an alternative to the conventional spectrogram and one of its main advantage is the ability to supply both resolution in time and frequency (Rao & Moharir, 1998). Basically, the complex Morlet wavelets, which are described as Gaussian-windowed complex sine waves, were layered over the pre-processed EEG data. Every complex wavelet includes a particular frequency. Following convolution, each frequency-specific distribution in frequency from 8 to 30 in 100 logarithmic steps was given a frequency representation. The squared magnitude of the convolution result was then used to extract power values at each time point. The former specifies a time frequency window with 100 frequency bins spaced out between 8 and 30 Hz, and the epoch of interest ranges from -1 to 4 seconds, or the stimulus's commencement. The number of ERS/ERD cycles is the key factor for the resolution in time and frequency. For a high resolution in time, a higher number of cycles is ideal. On the other hand, if the goal is to have a good resolution in frequency, the number of cycles should be low. In this way, 10 cycles ensures good resolution in both time and frequency.

5.2.2. Main Analysis

As mentioned before, the stimuli set of images is divided in two groups: images taken by presumptuous residents and tourists as explained in section 4.4.2.

The aim is to see if the popularity feature can work as a predictor and to verify the differences, in time-frequency, between the images of residents and tourists.

5.2.2.1. Loading and Epoching

First of all, the datasets that were pre-processed, as described in subchapter 5.1., were loaded using *pop_loadset* (Delorme & Makeig, 2004) function.

Then, the datasets were epoched from -1 to 4 seconds, being the $t = 0$ the moment when the image appears on the screen, employing for that *pop_epoch* (Delorme & Makeig, 2004) function.

5.2.2.2. Detection and Removal of Bad Trials

After loading and epoching, it is important to look at the EEG data and see if it is necessary to delete any epoch. The epochs with reaction times less than one second were disregarded from the analyses in an effort to achieve a uniform attentional and contemplative response in the data.

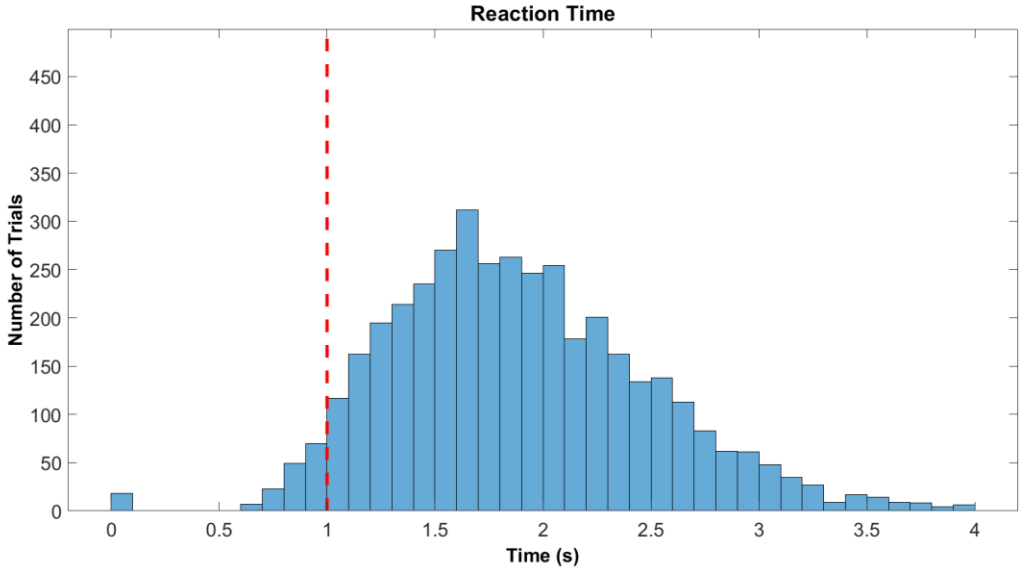

***Figure 5.3**: Histogram of reaction times for all trials. The red dotted line represents the boundary between good and bad trials, based on the reaction time criteria.*

As visible in **Figure 5.3**, there are some trials that must be deleted: the ones on the left side of the dotted red line, because we wanted to keep one fully second of contemplation of the image displayed.

For that, the *pop_select* (Delorme & Makeig, 2004) function was used to delete the correspondent trials with less than 1 second. The histogram obtained after this is represented in **Figure 5.4**.

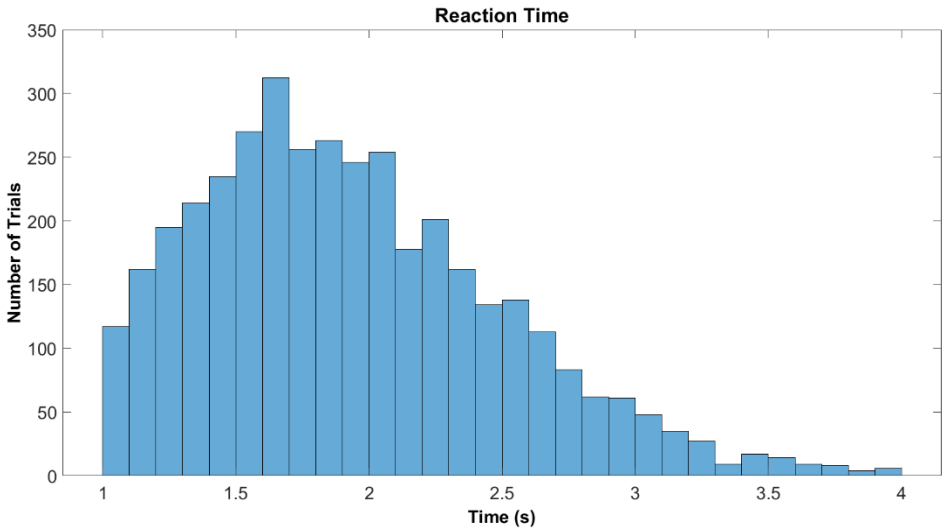

***Figure 5.4**: Histogram with the number of trials based on the reaction time after removing bad trials.*

Also, it is important to delete the epochs by frequency, meaning the rejection of bad trials for pre-selected independent components. For that, *rejectTrialSTFT* (Delorme & Makeig, 2004) function is used, which basically computes short-time Fourier Transform (STFT), using a rectangular window, within the frequency range of 1 to 30 Hz. Basically, each epoch is converted to one power spectral density time point. Then, the sum of power of the frequency band is converted into z-score and the epochs with more than 3 std are rejected.

5.2.2.3. ERS/ERD and Statistical Mask

After this, a time-frequency domain plot was created for all trials from all participants, excluding the deleted ones, using the electrodes from the frontal cortex. For that, 10 cycles ERS/ERD were used, which means that the observed ERS or ERD occurred in a period of ten cycles of the frequency bin (frequency of the particular morlet wavelet).

The datasets were epoched from -1 to 4 s. After obtaining time-frequency representation through wavelet functions, the time range was reduced as -500 ms (baseline limit period) to 4000 ms, to avoid the edge artifact effects by the wavelet convolution with the signal at the beginning and end of the window. This is caused by convolution and makes the time-frequency edges very noise. Thus, the time-frequency window must be reduced for a better visualization.

To better visualize the spots in time-frequency with marked ERS or ERD, a statistical mask was applied, which identifies significant spots based on some parameters, such as: baseline, frequency band, wavelet length and alpha level. This statistical mask is based on the t-test. Basically, t-test is used in this case to see if two groups have or do not have the same mean (meaning if they differ from each other), being known as independent two-sample t-test (*The T-Test | Introduction to Statistics | JMP*, 2023). After applying the test, when the p-value (change of making a wrong decision) is minor than alpha (0.05

in this case), it means that the two populations are statistically different (Kim, 2015). To apply the statistical mask is used the Bonferroni correction, in which the time-frequency representation obtained is utilized. The Bonferroni correction is used, because multiple comparisons are made, meaning that the several pixels of the time-frequency representation between 0 and 3500 ms are compared to the baseline. When that comparison is significant, the pixel receives the value 1, otherwise the value attributed is 0.

5.2.2.4. Comparison Between Images

First of all, each trial was processed and labelled according its belonging group (resident or tourist). This was done for subsequent identification and classification, facilitating their use in following tests.

To compare the tourist and resident images, a violin boxplot was created (see section 6.3) with ERS/ERD (%) values. It is important to note that this mentioned plot was created for all the significant spots found.

5.2.2.5. Popularity and ERS/ERD

After this, the popularity feature of the images was used to study the potential of ERS/ERD (%) as predictor of popularity. Therefore, the Spearman's correlation coefficient was used to study the correlation between popularity and ERS/ERD. Spearman's correlation coefficient is a measure of strength of a monotonic relationship between two different types of data (*Spearman's Correlation,* n.d.). This coefficient varies between -1 and 1 and the closer the coefficient is to ±1, with -1 to identify inverse correlation, and +1 for direct correlations.

In this way, the Spearman's correlation coefficient was used to analyse the relation between ERS/ERD and popularity for the significant spots discovered.

6. Results

The upcoming chapter, displays the several results obtained from the data analysis namely the time-frequency and its statistical analysis. First of all, it is going to be displayed the time-frequency plot for all participants and its statistical mask. Also, the plots for each significant spot are going to be displayed, to compare the resident and tourist populations and analyse the correlation between ERS/ERD (%) and popularity feature.

6.1. EEG Electrodes

The cortex region of interest is the frontal area, which includes the medial prefrontal cortex, because the frontal cortex is responsible for most of human decisions. Therefore, the electrodes choosen to analyse were: 'E38', 'E39', 'E40', 'E36', 'E35', 'E34', 'E33', 'E28', 'E29', 'E19', 'E22', 'E11','E12','E13','E14','E15', 'E3', 'E4', 'E5','E21', 'E20', 'E27', 'E26'. The electrodes of interest are represented in **Figure 6.1**.

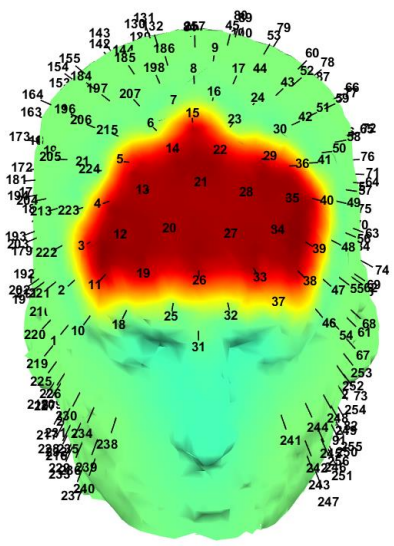

***Figure 6.1**: Frontal cortex - electrodes of interest.*

6.2. Time-Frequency

First of all, the time-frequency plot for all participants and all conditions was obtained, using 10 cycles of ERS/ERD. The plot is displayed in **Figure 6.2**.

To visualize better the significant time-frequency spots, a statistical mask was then applied, being the results displayed in **Figure 6.3**.

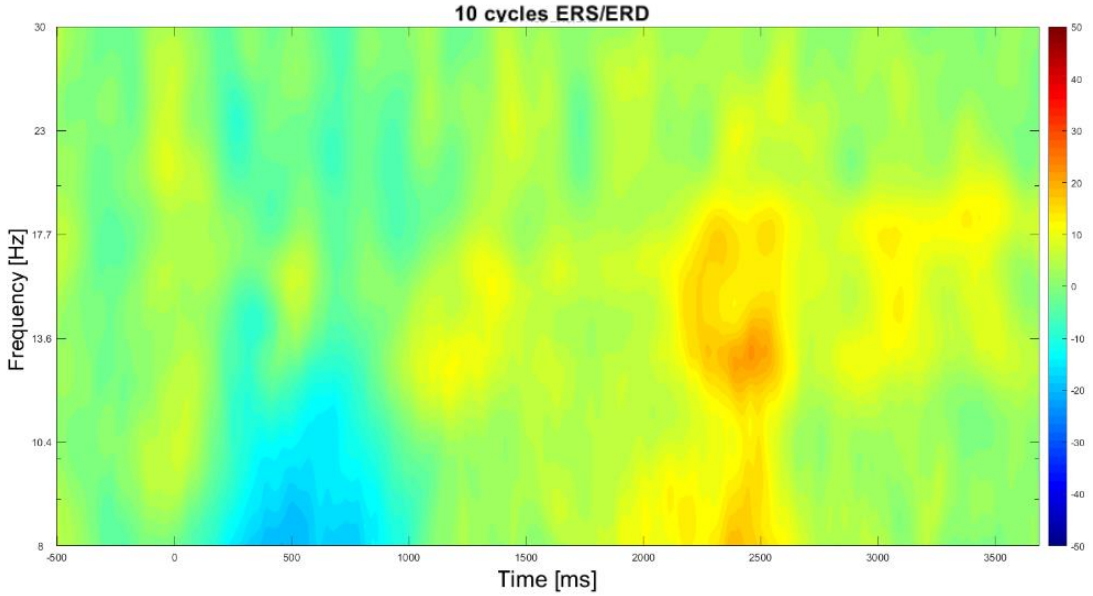

***Figure 6.2**: Time-frequency plot for all participants and all conditions. 10 cycles ERS/ERD was used. Frequency is in logarithmic scale.*

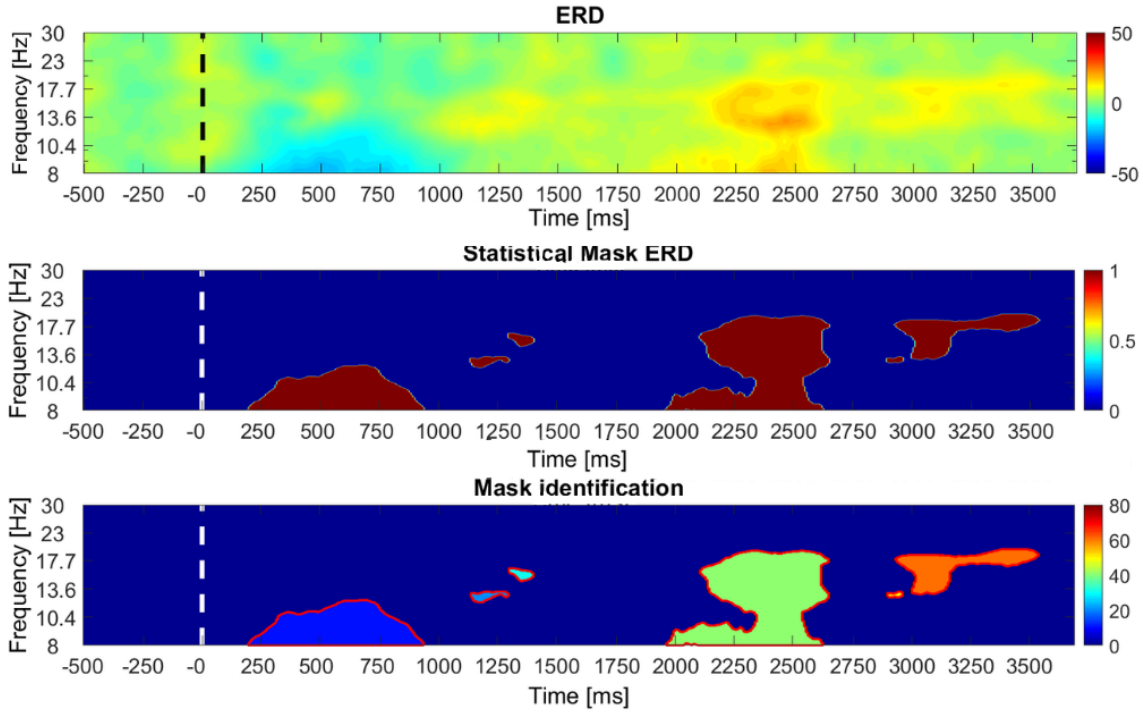

***Figure 6.3**: ERS/ERD plot (upper), statistical mask (middle) and mask identification (lower). Frequency is in logarithmic scale.*

As visible in **Figure 6.3**, after applying the statistical mask, there are a few significant time-frequency spots. Namely, it is clear that there are three main spots. Therefore, a new mask identification graphic with only those 3 spots (**Figure 6.4**) was then plotted.

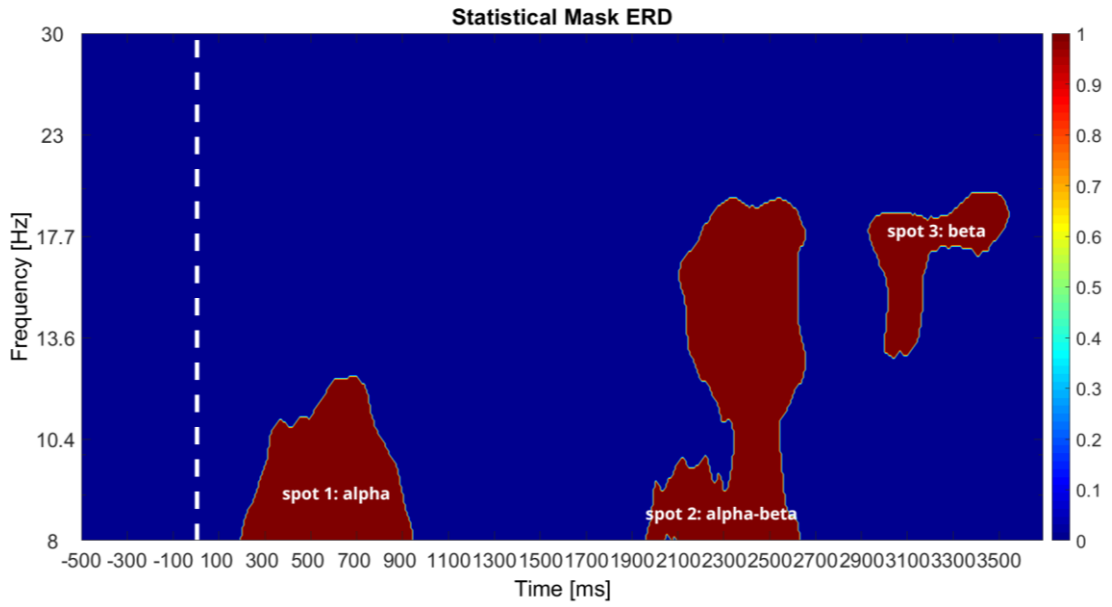

***Figure 6.4**: Statistical mask applied on ERS/ERD time-frequency and identification of the significant spots. Frequency is in logarithmic scale.*

Figure 6.4 suggests three time-frequency spots statistically significant: one in the alpha band, one in alpha and beta band and another one in the beta band. From now on, these three significant spots will be named as: spot 1 – the one in the alpha band; spot 2 – the alpha and beta; and spot 3 – the beta band.

6.3. Significant Spots Analysis

To address the main research question (1) – Can spectrum analysis of EEG signals be used to accurately represent the popularity of environments? If so, how is the relation between brain activity and popularity of environments described? –, it is possible to use two images' features: views and popularity. However, they represent the same, except that popularity is a normalized version based on the maximum views that each photographer had. Therefore, it will be only used the popularity feature.

In this subchapter, the results for the three significant spots regarding the popularity feature and the tourist vs resident comparison are displayed.

6.3.1. Spot 1: Alpha

First, a violin boxplot for each image group was created, so that the data visualization is easier. As **Figure 6.5** evidences that the resident images have greater concentration of values along lower ERS/ERD (%) than tourist pictures, as the density plot shows. This is corroborated by the average values of each group displayed in the middle of the boxplot. The p-value of $p = 0.87$ obtained, with 5% significance level, suggests that the two groups are not statistically different. In the resident images there are a couple of outliers, as well as in tourist images.

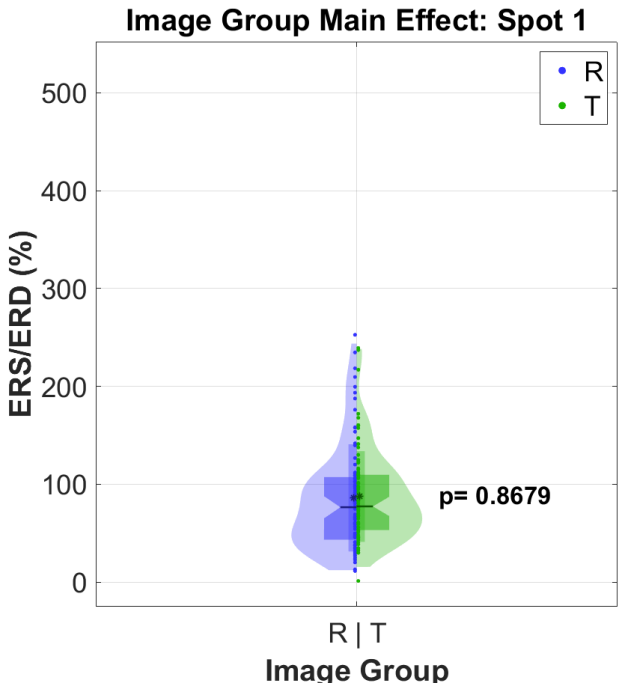

***Figure 6.5**: Violin boxplot for resident (blue) and tourist (green) groups for alpha spot.*

Finally, the Spearman's correlation coefficient was used to analyse the relation between ERS/ERD (%) and the popularity feature (**Figure 6.6**).

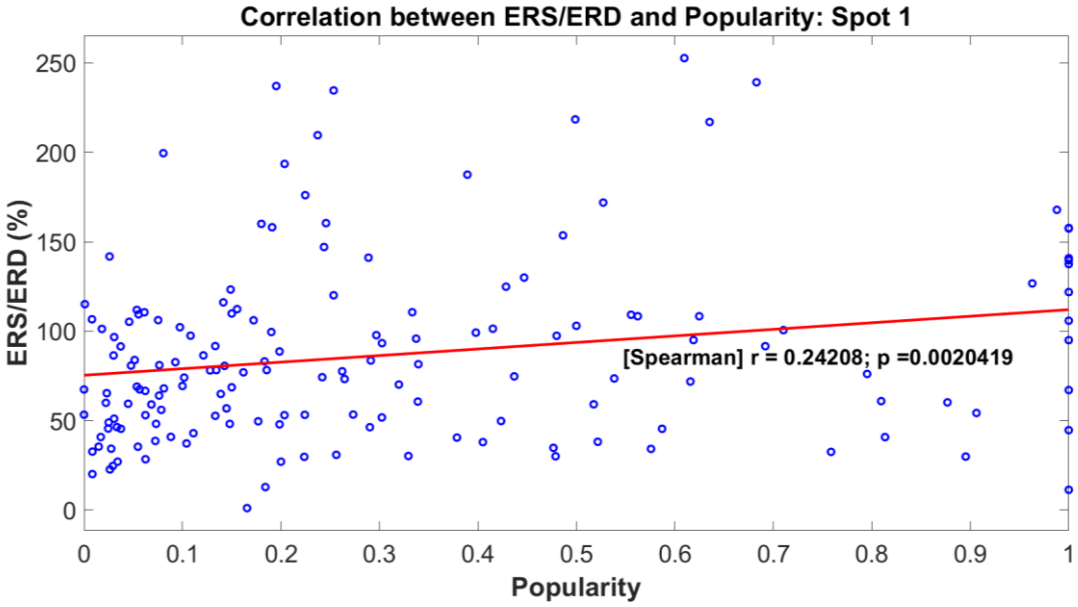

***Figure 6.6**: Spearman's correlation between ERS/ERD (%) and popularity for alpha spot.*

With this previous plot, there are two things to analyse: the value of the Spearman's coefficient and the p-value. When the Spearman's coefficient is bigger than 0, the relationship is monotonic positive, which is what happens ($r = 0.24$). As for the p-value, this feature has a value minor than 0.05, meaning that the null hypothesis (H0: there is no correlation between the two variables) can be rejected.

6.3.2. Spot 2: Alpha-Beta

Firstly, a violin boxplot shown in **Figure 6.7** was generated. Resident photos typically exhibit higher values of ERS/ERD (%) for the alpha-beta spot, which means a greater concentration of values along upper ERS/ERD (%) than tourist pictures, as visible in the density plot. The average values of each group, which are shown in the boxplot's centre, support this. As shown in the same preceding figure, there are a few outliers in both populations. With a 5% level of significance, the derived p-value of $p = 0.30$ indicates that there is not a statistical difference between the two groups.

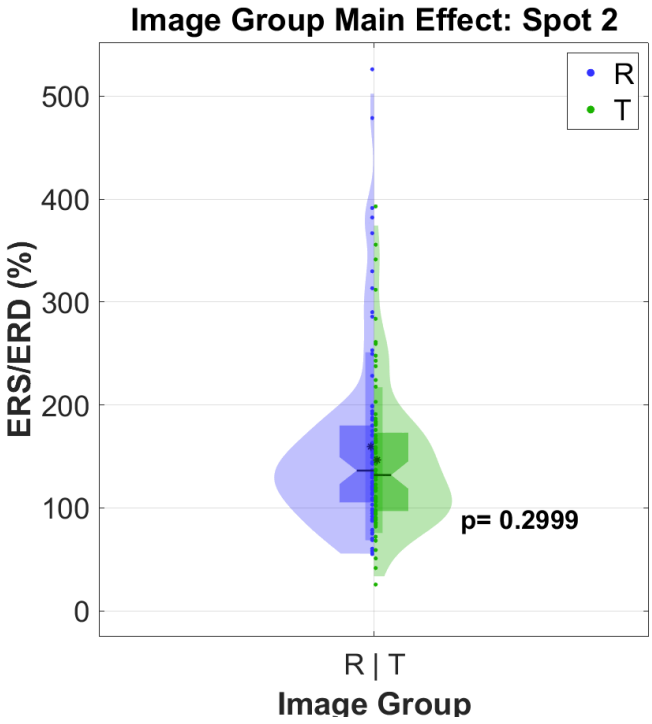

***Figure 6.7**: Violin boxplot for resident (blue) and tourist (green) groups for alpha-beta spot.*

Lastly, the relationship between ERS/ERD (%) and the popularity attribute was examined using the Spearman's correlation coefficient. Once again, the Spearman's coefficient is greater than 0 ($r = 0.07$), which indicates that the relationship is monotonically positive. For the p-value, this value is $p = 0.40$.

6.3.3. Spot 3: Beta

First, violin boxplot was created. For beta region, tourist images evidence higher ERS/ERD (%) values as shown in **Figure 6.8**. Once more, there are few outliers in both groups. At the 5% level of significance, the obtained p-value of $p = 0.54$ shows that there is not a statistical difference between the resident and tourist images.

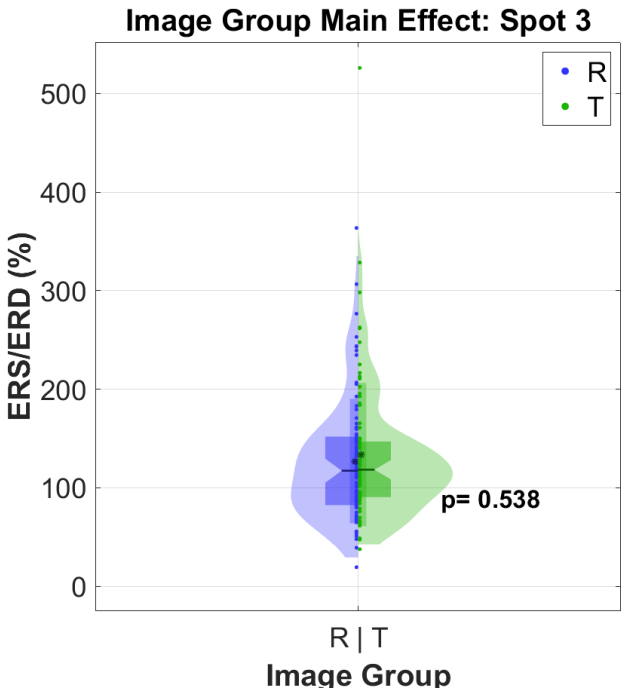

***Figure 6.8**: Violin boxplot for resident (blue) and tourist (green) groups for beta spot.*

At least, the relationship between ERS/ERD (%) and the popularity feature was examined using the Spearman's correlation coefficient. For beta band, the Spearman's coefficient is positive $r = 0.05$, which indicates a positive monotonic relation between ERS/ERD (%) and popularity. Regarding the p-value, it is $p = 0.56$.

7. Discussion

7.1. Time-Frequency

All the selected electrodes for time-frequency analysis belong to the frontal cortex, because this brain region is important in certain aspects for the BAP study. The frontal cortex includes important brain areas described in subchapter 2.4, such as: nucleus accumbens (crucial in functions like pleasure and emotions), medial prefrontal cortex (important in functions, such as: decision-making process) and anterior cingulate cortex (crucial in functions like cognitive and emotion processing).

By applying the wavelet method described by (Cohen, 2014), a time-frequency plot shown in the **Figure 6.2** with all trials from all participants (excluding the bad trials) was created. For this plot, 10 cycles were used to guarantee a good resolution both in time and in frequency. By analysing **Figure 6.2** with naked eye, it is clear the presence of 2 significant spots after $t = 0\ s$ (image display): one around 500 ms and another one around 2500 ms. The first one is linked to an event-related desynchronization as suggested by the bluish colours. Regarding the second, it is linked to an event-related synchronization as visible by the orange colours.

In order to have a clear knowledge of the significant spots, a statistical mask was applied to the time-frequency plot. This consists in creating a binary mask and multiplying it by the original dataset element-wise. Each data point will be assigned a value of either 1 (significant) or 0 (non-significant). After applying the mask, **Figure 6.3** was obtained, which includes 3 subplots: the upper subplot is the same one from **Figure 6.2**; the middle subplot is the plot acquired from the application of the statistical mask; and the lower subplot is the same one from the middle plot but with colours to identify the different spots. From this mask application, it is clear the presence of 3 main spots. The statistical mask identification was then plotted in **Figure 6.4** to have a clear visualization. These 3 significant spots are from now on named accordingly to the frequency band of belonging: spot 1 is alpha spot, spot 2 is alpha-beta spot, and spot 3 is beta spot.

These 3 identified significant spots are related to different events. The alpha band is linked to the visual stimuli: this means that the ERD seen in the plot is a consequence of the neuronal response time to visual stimuli in the frontal area (Bullier, 2001). After this, the frontal cortex becomes more active and involved in the decision-making process (Klein-Flügge et al., 2022). Therefore, the alpha-beta and beta band spots are due to the decision-making and rating process.

When mentioning ERS and ERD, some studies, such as (Pfurtscheller, 2001) refer that ERD is related to an activation of cortical area, whereas ERS is associated with deactivation (inhibition) of a cortical area. Thus, the obtained alpha spot represents an activation of the cortical neurons, which is a characteristic of visual processing (Pfurtscheller, 2001) that occurs mainly in the alpha band. The last 2 spots are characterized by a deactivation state, which means that the information processing is reduced (Pfurtscheller, 2001) in the frontal cortex. These findings suggest that the subject shows more attention in the beginning of each trial when they receive the visual stimuli.

7.2. Significant Spots Analysis

In this subchapter it will be discussed the results from the 3 significant spots, regarding the resident vs tourist comparison and the popularity feature.

7.2.1. Spot 1: Alpha

As seen in **Figure 6.2**, this significant spot is marked by ERD, which reflects a decrease in alpha power, the so-called alpha suppression (Bacigalupo & Luck, 2022). This means that when the subject is with their eyes open and processing the visual information, the alpha brain waves tend to decrease in power. This is a typical EEG behaviour in a visual stimuli EEG experiment.

To begin with the resident vs tourist analysis, a violin boxplot was generated with both groups on it, as seen in **Figure 6.5** and reproduced in **Figure 7.1**.

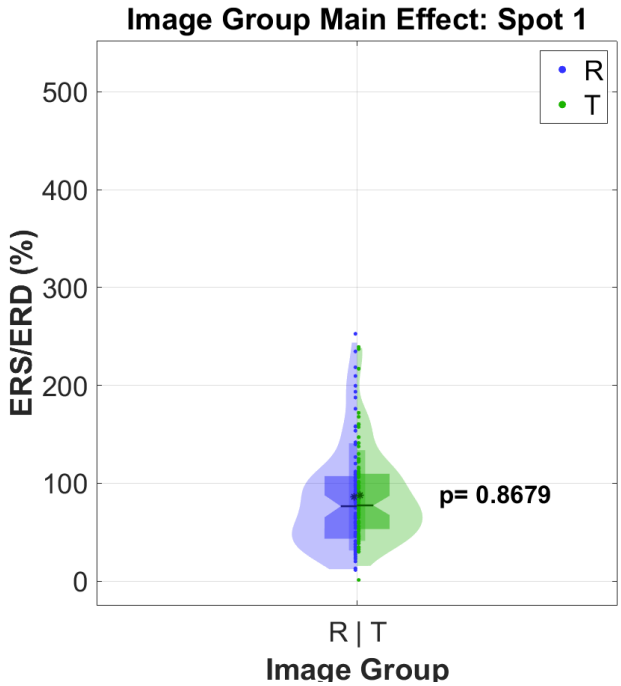

***Figure 7.1**: Violin boxplot for resident (blue) and tourist (green) groups for alpha spot.*

By comparing the black line of both boxplots, which indicates the median, it is clear that the first 50% values of tourist's images are greater than the first 50% values of the resident's images. However, the values from the tourist's pictures are compacted in a shorter range of values, as interquartile ranges indicate (ampoule shape). This shows that the resident group has the data more dispersed. The density plot suggests that there is a higher probability of finding values near the median, than in the first and fourth quartiles, for both populations. Regarding the outliers, it is clear that the resident population has one more outlier than the tourist group. The p-value displayed of $p = 0.87$ indicates that the null hypothesis (which usually declares that there is no difference or effect) cannot be rejected, meaning that the two populations are statistically identical.

Then, to study the popularity feature as a predictor, the Spearman's correlation coefficient was used and plotted (**Figure 6.6**) the two variables ERS/ERD and popularity. The value for the Spearman correlation coefficient obtained was of $r = 0.24$. According to (Leclezio et al., 2015) this value indicates a weak relationship between ERS/ERD and popularity. The p-value is $p < 0.05$, and states the significance of the relation between the two variables, meaning that the relationship discovered is likely to be real.

It is also important to state that the alpha band is associated with several brain functions important to the experiment, such as: cognition, attention and task engagement (Buskila et al., 2019; Hohaia et al., 2022).

To sum up, this significant spot in alpha band is a reflexion of alpha suppression caused by the attention paid by the subject when receiving the visual stimuli. In this case, ERS/ERD can be used as a predictor of popularity (monotonic positive relation), despite the fact of the weak r value obtained between both $r = 0.24$.

7.2.2. Spot 2: Alpha-Beta

First, we should analyse the differences between resident and tourist populations. By taking a look at the violin boxplot displayed in **Figure 6.7** and reproduced in **Figure 7.2**, it seems that both populations have similar median values. However, the resident group has a slightly greater median value, as the black line indicates. This means that the first 50% of the values of the tourist group are lower that the resident population. Also, the ampoule shape of the plot suggests that the interquartile values of the resident group is slightly greater than the tourist population, which means that the resident pictures evoke slightly bigger ERS/ERD (%) than the tourist ones. The distribution's form, which is very narrow on either end and wide in the middle, suggests that the values are more concentrated in a small area around the median. Regarding the interquartile range, it is clear that is similar for both populations. Therefore, the data has dispersion degree identical in both groups. As for the outliers, the resident group shows more outliers than the tourist population. The p-value found is $p = 0.30$ states that with $\alpha = 5\%$ the null hypothesis of both populations being statistically identical cannot be rejected.

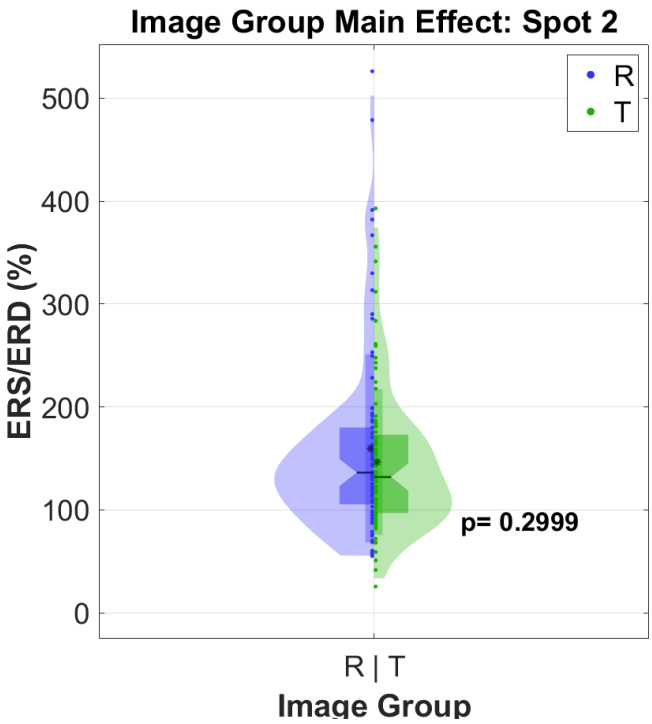

***Figure 7.2**: Violin boxplot for resident (blue) and tourist (green) groups for alpha-beta spot.*

After this, the popularity feature was used to see if ERS/ERD (%) could be used as a predictor of popularity. For that, the Spearman correlation coefficient was used to study the relationship between the two previous variables. The Spearman correlation coefficient obtained was $r = 0.07$. In compliance with (Leclezio et al., 2015) there is no relation between ERS/ERS (%) and popularity or it is negligible. The p-value for this coefficient is $p = 0.40$. Since the p-value is bigger than $\alpha = 5\%$, this means that the evidence for rejecting the null hypothesis (H0: there is no correlation between the two variables) is very weak to none, which means that there is no correlation between ERS/ERD (%) in the alpha-beta spot. Therefore, ERS/ERD (%) cannot be used as a predictor of popularity for the alpha-beta band.

7.2.3. Spot 3: Beta Band

The comparison between resident and tourist pictures was firstly made by building the violin boxplot in **Figure 6.8** and reproduced in **Figure 7.3**. By naked eye, it seems once again that both populations have an identical mean value. However, the tourist group has a higher median value (confirmed by the black line), which indicates that the tourist population has its first 50% data points with values bigger than the resident group. Regarding the interquartile range, it is shorter, as seen in the ampoule's shape – the values of the tourist group are more compacted. These two aspects have a direct effect on the violin boxplot: the values are more concentrated around the median and therefore, the density plot is bigger near the median value of the tourist population. These range values suggest that the resident group has a more dispersed data. Regarding the outliers, **Figure 7.3Figure 6.8** shows that the number of outliers is similar in both populations. The p-value of $p = 0.54$ obtained allows the conclusion that resident and tourist populations are statistically identical, because it is bigger than 0.05.

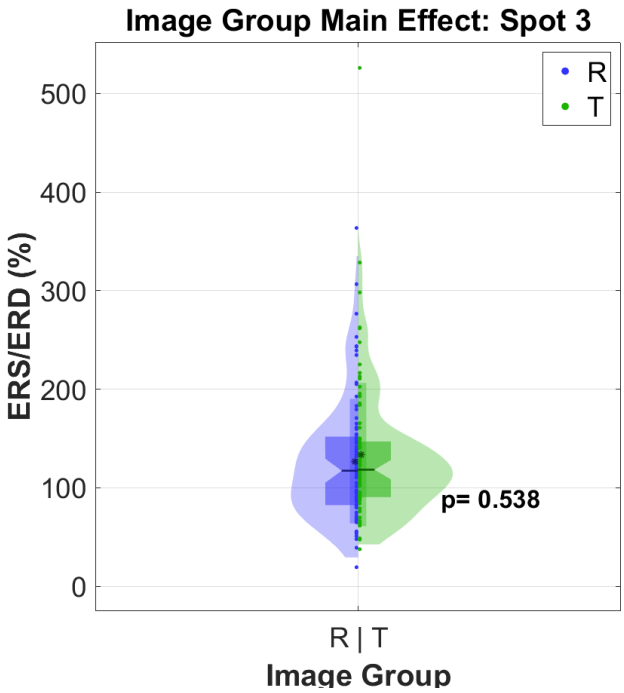

***Figure 7.3**: Violin boxplot for resident (blue) and tourist (green) groups for beta spot.*

Finally, the hypothesis of using ERS/ERD (%) as predictor of popularity was studied. In this way, the Spearman's correlation coefficient was used to analyse it. The value for the Spearman coefficient obtained was $r = 0.05$, which according to (Leclezio et al., 2015) means that either there is no relation between the two variables either the relation is negligible. The p-value acquired for the Spearman correlation was of $p = 0.56$, meaning that the Spearman coefficient could have no significance. In other words, there is a chance that the negligible relation between ERS/ERD (%) and popularity could be false.

ERS/ERD (%) cannot be utilized as a predictor of popularity for the beta band, despite the possibility that the p-value suggests a spurious relationship between ERS/ERD (%) and popularity.

7.3. Comparison with the Literature

Regarding the use of ERS/ERD (%) as predictor of popularity, this relation can be established for the alpha band. When looking to (Berns & Moore, 2012) study, they reached a result of $r = 0.32$ for the correlation between nucleus accubens activity and the number of albums sold containing song, which is a moderate correlation according to (Leclezio et al., 2015). When comparing this value with the one obtained in the alpha band ($r = 0.24$) of BAP experiment, it is clear that there is not big difference between them, which supports the idea that ERS/ERD (%) can be used as a predictor of popularity for the alpha band. As for alpha-beta and beta bands, as the values obtained are too low, the last statement cannot be true.

The (Dmochowski et al., 2014) study showed bigger values of r ($r = 0.4$ (tweet rate) for the first experiment; $r = 0.81$ ($population\ rating$) and $r = 0.51$ (sample rating) for the second experiment). This means a stronger relation between the variables.

These two studies (Berns & Moore, 2012; Dmochowski et al., 2014) applied some models to analyse the data and tried to predict cultural popularity with brain activity.

The key difference in my study is the appliance of brain as predictor methodology to neurourbanism features – trying to predict the popularity of an urban image with ERS/ERD (%).

Regarding (Zhu et al., 2021), the experiment is already in the neurourbanism area. However, one of the goals was to see if the characteristics of the urban environments were related to emotions. They reached the conclusion that there are relations between urban environment and some emotions and, for instance, there is no relation between public transit and the seven basic emotions (happiness, surprise, contempt, sadness, fear, disgust, and anger). Therefore, the results obtained in (Zhu et al., 2021) study are related to this work, exposing that urban stimuli can be depicted via brain responses.

As for the (Mavros et al., 2022) study, it is incorporated in the neurourbanism area. Although, its goal is not trying to predict something, but to compare the experience of walking indoor and outdoor to analyse the physiological responses of the different urban environments. In this way, it cannot be directly compared with the BAP experiment, despite both projects having the same theme – neurourbanism.

8. Conclusion

8.1. Time-Frequency

Starting with the time-frequency, by applying the wavelet method a plot in time-frequency domain was generated for all trials (except the bad ones) of all participants, using the frontal cortex electrodes. To ensure a good resolution in time and in frequency, the plot was built with 10 cycles ERS/ERD. In order to discover the significant spots in the time-frequency plot, a statistical mask was applied, which allowed the conclusion of the presence of three significant spots: one in alpha band (spot 1), one in alpha-beta band (spot 2) and another one in beta band (spot 3).

These significant spots are linked to each moment of the visual processing in the human brain. The spot 1 is related to visual stimuli, meaning when the subject sees the image. This spot is characterized by ERD, which means the activation of the cortical area – one trait of the visual processing in alpha band.

The spots 2 and 3 are linked to the decision-making process of scoring the picture. During this part of the trial, the information processing is reduced in the frontal cortex, which is reflected in a deactivation of the same cortical area – presence of ERS.

8.2. Significant Spots Analysis

Regarding the alpha band spot, by seeing the boxplot and violin boxplot the tourist's median is higher than the resident's, whereas the interquartile range is more compacted in the tourist group. These findings indicate that the tourist population has higher values of ERS/ERD (%), which means the inhibition of specific brain processes or the diversion of attention from the targeted stimulus for this population, and less dispersed data. The p-value acquired with these plots ($p = 0.87$) suggests that resident and tourist populations are not statically different. The popularity feature was then used to study its relation with ERS/ERD by using the Spearman correlation coefficient and for that the $r = 0.24$ evidences a weak relation between both variables. This spot is marked by alpha suppression that is caused when the subject is processing the visual information received.

As for the alpha-beta spot, both plots generated show that the resident population has a slightly bigger median value and that both groups have similar interquartile range values. These observations evidence that the resident group has higher values of ERS/ERD (%) – this refers to the rerouting of attention away from the targeted stimulus for this group or the inhibition of particular brain processes – , and both groups have similar dispersion degree. The p-value obtained with these plots $p = 0.30$ indicates that there are not statistical differences between the resident and tourist populations. Using the Spearman correlation coefficient, the popularity feature's relationship with ERS/ERD was then examined, and the resultant $r = 0.07$ indicates that there is no association between both or the relation can be negligible.

The tourist population has a little larger median value than the non-resident population, and the resident group has a bigger interquartile range, according to both plots created for the beta band. These findings show that the resident group has its data more dispersed than the tourist population, and that the resident tourist has greater values of ERS/ERD (%), which relates to the rerouting of attention away

from the focused stimulus for this group or the inhibition of specific brain processes. These plots' p-value of $p = 0.54$ shows that there are not statistical disparities between the resident and tourist populations. The relationship between the popularity characteristic and ERS/ERD was then investigated using the Spearman correlation coefficient, and the resultant $r = 0.05$ suggests that there is either no association between the two variables or that the relationship may be insignificant.

By comparing the ERS/ERD (%) values of the three significant spots, it is possible to state that the first and last spots have bigger ERS/ERD (%) values in the tourist population, and the second spot has the opposite behaviour. This means that in the alpha and beta bands, the tourists' pictures cause a bigger deactivated state with reduced information process, and in the alpha-beta band the same happens with the resident population. Also, by analysing the p-values, it is known that the bigger the p-value is the similar are the mean values of each group. In this way, it is possible to state that the populations are more similar in the alpha band and closer to be statistically different in the alpha-beta band.

Regarding the ability of ERS/ERD (%) being used as a predictor of popularity of the images, it is possible to affirm that alpha time-frequency spot can be used as a predictor.

8.3. Future Work

During the present work, I came up with some ideas of what could be done further up to improve this EEG spectral analysis. First, it would be interest to study other image's features to find a possible strong relation between ERS/ERD (%) and that feature. One feature that I would use could be the green index, in order to investigate if the EEG spectral analysis could be a predictor of the degree of vegetation present in the images.

Also, in addition to analyse the differences between the resident and tourist images, the differences, in time-frequency, for the different scores could be studied. This means that the 4 possible scores that the subjects can use, would be grouped in 4 different populations and studied their differences. With these four populations, it would be interest to see if it is possible to predict the participants' score based on their brain activity, bringing a new insight into the data.

Besides the EEG spectral analysis, it would be interesting to use brain connectivity to see if it could be used as a predictor of popularity too. Different connectivity measures could be used and see if they could be used as a predictor of popularity of the pictures. For example, by using functional connectivity, it would be possible to analyse temporal correlations between the different EEG channels and possibly identify certain patterns of synchronized brain activity. These patterns could be a predictor variable of the images' popularity, for instance.

Finally, it would also be a great idea to test machine learning models. Using different classification models to see if based on brain activity these models could predict the popularity of the images displayed.

9. References

Adli, M., Berger, M., Brakemeier, E.-L., Engel, L., Fingerhut, J., Gomez-Carrillo, A., Hehl, R., Heinz, A., Mayer, J., & Mehran, N. (2017). Neurourbanism: towards a new discipline. *The Lancet Psychiatry*, *4*(3), 183–185.

Aguiar-Conraria, L., & Soares, M. J. (2014). The continuous wavelet transform: Moving beyond uni-and bivariate analysis. *Journal of Economic Surveys*, *28*(2), 344–375.

Alexander, W. H., & Brown, J. W. (2011). Medial prefrontal cortex as an action-outcome predictor. *Nature Neuroscience*, *14*(10), 1338–1344.

Al-Fahoum, A. S., & Al-Fraihat, A. A. (2014). Methods of EEG signal features extraction using linear analysis in frequency and time-frequency domains. *International Scholarly Research Notices*, *2014*.

Ancora, L. A., Blanco-Mora, D. A., Alves, I., Bonifácio, A., Morgado, P., & Miranda, B. (2022). Cities and neuroscience research: A systematic literature review. *Frontiers in Psychiatry*, *13*, 983352.

Bacigalupo, F., & Luck, S. J. (2022). Alpha-band EEG suppression as a neural marker of sustained attentional engagement to conditioned threat stimuli. *Social Cognitive and Affective Neuroscience*, *17*(12), 1101–1117.

Berger, A. (2002). How does it work?: Magnetic resonance imaging. *BMJ: British Medical Journal*, *324*(7328), 35.

Berns, G. S., & Moore, S. E. (2012a). A neural predictor of cultural popularity. *Journal of Consumer Psychology*, *22*(1), 154–160.

Berns, G. S., & Moore, S. E. (2012b). A neural predictor of cultural popularity. *Journal of Consumer Psychology*, *22*(1), 154–160. https://doi.org/10.1016/j.jcps.2011.05.001

Biasiucci, A., Franceschiello, B., & Murray, M. M. (2019). Electroencephalography. *Current Biology*, *29*(3), R80–R85.

Brain anatomy, Anatomy of the human brain | Mayfield Brain & Spine Cincinnati, Ohio. (2018). https://mayfieldclinic.com/pe-anatbrain.htm

Bressler, S. L., & Ding, M. (2006). Event-related potentials. *Wiley Encyclopedia of Biomedical Engineering*.

Bullier, J. (2001). Integrated model of visual processing. *Brain Research Reviews*, *36*(2–3), 96–107.

Bush, G., Luu, P., & Posner, M. I. (2000). Cognitive and emotional influences in anterior cingulate cortex. *Trends in Cognitive Sciences*, *4*(6), 215–222.

Buskila, Y., Bellot-Saez, A., & Morley, J. W. (2019). Generating brain waves, the power of astrocytes. *Frontiers in Neuroscience*, *13*, 1125.

Cerebral cortex: Structure and functions | Kenhub. (2023). https://www.kenhub.com/en/library/anatomy/cerebral-cortex

Chaurasiya, H. (2020). Time-frequency representations: spectrogram, cochleogram and correlogram. *Procedia Computer Science*, *167*, 1901–1910.

Cionek, J. (2020). Wet, dry, active and passive electrodes. What are they, and what to choose? *Brain Support*.

Cohen, M. X. (2014). *Analyzing neural time series data: theory and practice*. MIT press.

Cole, S. R., & Voytek, B. (2017). Brain oscillations and the importance of waveform shape. *Trends in Cognitive Sciences*, *21*(2), 137–149.

Collura, T. F. (1993). History and evolution of electroencephalographic instruments and techniques. *Journal of Clinical Neurophysiology*, *10*(4), 476–504.

Cooper, R., Osselton, J. W., & Shaw, J. C. (2014). *EEG technology*. Butterworth-Heinemann.

Dattola, S., Morabito, F. C., Mammone, N., & La Foresta, F. (2020). Findings about loreta applied to high-density eeg—a review. *Electronics*, *9*(4), 660.

Delorme, A., & Makeig, S. (2004). EEGLAB: an open source toolbox for analysis of single-trial EEG dynamics including independent component analysis. *Journal of Neuroscience Methods*, *134*(1), 9–21.

Di Flumeri, G., Aricò, P., Borghini, G., Sciaraffa, N., Di Florio, A., & Babiloni, F. (2019). The dry revolution: Evaluation of three different EEG dry electrode types in terms of signal spectral features, mental states classification and usability. *Sensors*, *19*(6), 1365.

Dmochowski, J. P., Bezdek, M. A., Abelson, B. P., Johnson, J. S., Schumacher, E. H., & Parra, L. C. (2014). Audience preferences are predicted by temporal reliability of neural processing. *Nature Communications*, *5*(1), 4567.

EEG ELECTRODES. (2017). http://eegget-it.nl/eeg_electrodes.html

EEG Systems compatible with MR and MEG environments. (2021). https://www.egi.com/research-division/eeg-systems/mr-compatible-eeg-systems

Electrical Geodesics, Inc. (2021). https://www.egi.com/

Etkin, A., Egner, T., & Kalisch, R. (2011). Emotional processing in anterior cingulate and medial prefrontal cortex. *Trends in Cognitive Sciences*, *15*(2), 85–93.

Euston, D. R., Gruber, A. J., & McNaughton, B. L. (2012). The role of medial prefrontal cortex in memory and decision making. *Neuron*, *76*(6), 1057–1070.

Falk, E. B., Berkman, E. T., Whalen, D., & Lieberman, M. D. (2011). Neural activity during health messaging predicts reductions in smoking above and beyond self-report. *Health Psychology*, *30*(2), 177.

Fett, A.-K. J., Lemmers-Jansen, I. L. J., & Krabbendam, L. (2019). Psychosis and urbanicity: a review of the recent literature from epidemiology to neurourbanism. *Current Opinion in Psychiatry*, *32*(3), 232.

Fibra óptica - InfoEscola. (n.d.). Retrieved April 20, 2023, from https://www.infoescola.com/fisica/fibra-optica/

fMRI Acquisition | NordicNeuroLab. (2023). https://www.nordicneurolab.com/product/fmri-acquisition

fMRI Response Grips | Social, Life, and Engineering Sciences Imaging Center. (2023). https://www.imaging.psu.edu/facilities/3t-mri/fmri-response-grips

Genevsky, A., Yoon, C., & Knutson, B. (2017). When brain beats behavior: Neuroforecasting crowdfunding outcomes. *Journal of Neuroscience*, *37*(36), 8625–8634. https://doi.org/10.1523/JNEUROSCI.1633-16.2017

Geodesic EEG System 400 series. (2021). https://www.egi.com/clinical-division/clinical-division-clinical-products/ges-400-series

GeoScan handheld sensor digitization. (2021). https://www.egi.com/research-division/electrical-source-imaging/geoscan-sensor-digitization

Gevins, A., Smith, M. E., McEvoy, L. K., Leong, H., & Le, J. (1999). Electroencephalographic imaging of higher brain function. *Philosophical Transactions of the Royal Society of London. Series B: Biological Sciences*, *354*(1387), 1125–1134.

Gogolla, N. (2017). The insular cortex. *Current Biology*, *27*(12), R580–R586.

Hargreaves, B., Worters, P. W., Pauly, K. B., Pauly, J. M., Koch, K. M., & Gold, G. E. (2011). Metal induced artifacts in MRI. *AJR. American Journal of Roentgenology*, *197*(3), 547.

Heimer, L., & Van Hoesen, G. W. (2006). The limbic lobe and its output channels: implications for emotional functions and adaptive behavior. *Neuroscience & Biobehavioral Reviews*, *30*(2), 126–147.

High-density electroencephalogram (HD-EEG) on Epilepsy and Tumor - Clinical Trials Registry - ICH GCP. (2023). https://ichgcp.net/clinical-trials-registry/NCT04266041

Hohaia, W., Saurels, B. W., Johnston, A., Yarrow, K., & Arnold, D. H. (2022). Occipital alpha-band brain waves when the eyes are closed are shaped by ongoing visual processes. *Scientific Reports*, *12*(1), 1194.

Holdsworth, S. J., & Bammer, R. (2008). Magnetic resonance imaging techniques: fMRI, DWI, and PWI. *Seminars in Neurology*, *28*(04), 395–406.

Human Brain: Facts, Functions & Anatomy | Live Science. (2021). https://www.livescience.com/29365-human-brain.html

Hyvarinen, A. (1999). Fast and robust fixed-point algorithms for independent component analysis. *IEEE Transactions on Neural Networks*, *10*(3), 626–634.

Hyvärinen, A., Karhunen, J., & Oja, E. (2001). *Independent Component Analysis*.

Jobson, D. D., Hase, Y., Clarkson, A. N., & Kalaria, R. N. (2021). The role of the medial prefrontal cortex in cognition, ageing and dementia. *Brain Communications*, *3*(3), fcab125.

Johnson, D. H. (2006). Signal-to-noise ratio. *Scholarpedia*, *1*(12), 2088.

Jorge, J., Van der Zwaag, W., & Figueiredo, P. (2014). EEG–fMRI integration for the study of human brain function. *Neuroimage*, *102*, 24–34.

Kalcher, J., & Pfurtscheller, G. (1995). Discrimination between phase-locked and non-phase-locked event-related EEG activity. *Electroencephalography and Clinical Neurophysiology*, *94*(5), 381–384.

Kim, T. K. (2015). T test as a parametric statistic. *Korean Journal of Anesthesiology*, *68*(6), 540–546.

Kirschstein, T., & Köhling, R. (2009). What is the source of the EEG? *Clinical EEG and Neuroscience*, *40*(3), 146–149.

Klein-Flügge, M. C., Bongioanni, A., & Rushworth, M. F. S. (2022). Medial and orbital frontal cortex in decision-making and flexible behavior. *Neuron*.

Knutson, B., & Genevsky, A. (2018). Neuroforecasting Aggregate Choice. *Current Directions in Psychological Science*, *27*(2), 110–115. https://doi.org/10.1177/0963721417737877

Kolling, N., Behrens, T. E. J., Wittmann, M. K., & Rushworth, M. F. S. (2016). Multiple signals in anterior cingulate cortex. *Current Opinion in Neurobiology*, *37*, 36–43.

La Vaque, T. J. (1999). The history of EEG hans berger: psychophysiologist. A historical vignette. *Journal of Neurotherapy*, *3*(2), 1–9.

Lattari, E., Velasques, B., Paes, F., Cunha, M., Budde, H., Basile, L., Cagy, M., Piedade, R., Machado, S., & Ribeiro, P. (2010). Corticomuscular coherence behavior in fine motor control of force: a critical review. *Rev. Neurol*, *51*(10), 610–623.

Leclezio, L., Jansen, A., Whittemore, V. H., & de Vries, P. J. (2015). Pilot validation of the tuberous sclerosis-associated neuropsychiatric disorders (TAND) checklist. *Pediatric Neurology*, *52*(1), 16–24.

Logothetis, N. K. (2008). What we can do and what we cannot do with fMRI. *Nature*, *453*(7197), 869–878.

Lopez-Gordo, M. A., Sanchez-Morillo, D., & Valle, F. P. (2014). Dry EEG electrodes. *Sensors*, *14*(7), 12847–12870.

Lu, S., Phung, B. T., & Zhang, D. (2018). A comprehensive review on DC arc faults and their diagnosis methods in photovoltaic systems. *Renewable and Sustainable Energy Reviews*, *89*, 88–98. https://doi.org/10.1016/j.rser.2018.03.010

Luck, S. J. (2012). Event-related potentials. *APA Handbook of Research Methods in Psychology, Vol. 1. Foundations, Planning, Measures, and Psychometrics* , 523–546.

Matlab, S. (2012). Matlab. *The MathWorks, Natick, MA*.

Matloff, N. (2011). *The art of R programming: A tour of statistical software design*. No Starch Press.

Mavros, P., J Wälti, M., Nazemi, M., Ong, C. H., & Hölscher, C. (2022). A mobile EEG study on the psychophysiological effects of walking and crowding in indoor and outdoor urban environments. *Scientific Reports*, *12*(1), 18476.

McFarland, D. J., Miner, L. A., Vaughan, T. M., & Wolpaw, J. R. (2000). Mu and beta rhythm topographies during motor imagery and actual movements. *Brain Topography*, *12*, 177–186.

Moreira, C. (2015). Potencial de ação. *Revista de Ciência Elementar*, *3*(4).

Morley, A., Hill, L., & Kaditis, A. G. (2016). 10-20 system EEG Placement. *European Respiratory Society, European Respiratory Society*.

MR Ingenia Elition 3.0T | Philips. (2023). https://www.usa.philips.com/healthcare/resources/landing/the-next-mr-wave/ingenia-elition

Muhammad, G., Hossain, M. S., & Kumar, N. (2020). EEG-based pathology detection for home health monitoring. *IEEE Journal on Selected Areas in Communications*, *39*(2), 603–610.

Nayak, C. S., & Anilkumar, A. C. (2020). *EEG Normal Waveforms. StatPearls*. Treasure Island, FL: StatPearls Publishing. http://www. ncbi. nlm. nih. gov ….

Net Station Acquisition for Routine EEG data collection: Video Tutorial. (2021). https://www.egi.com/knowledge-center/item/61-net-station-acquisition-for-routine-eeg-collection

Oldendorf, W., Oldendorf, W., Oldendorf, W., & Oldendorf, W. (1988). Advantages and Disadvantages of MRI. *Basics of Magnetic Resonance Imaging*, 125–138.

Pelli, D. G., & Vision, S. (1997). The VideoToolbox software for visual psychophysics: Transforming numbers into movies. *Spatial Vision*, *10*, 437–442.

Pereira, L., & Neto, L. (2014). *Núcleo accumbens humano : da anatomia à imagiologia e clínica*. https://repositorio.ul.pt/handle/10451/17947

Pfurtscheller, G. (2001). Functional brain imaging based on ERD/ERS. *Vision Research*, *41*(10–11), 1257–1260.

Pfurtscheller, G., & Da Silva, F. H. L. (1999). Event-related EEG/MEG synchronization and desynchronization: basic principles. *Clinical Neurophysiology*, *110*(11), 1842–1857.

Plonsey, R., Barr, R. C., & Bioelectricity, A. (2007). *Quantitative Approach*. Springer.

Pykett, J., Osborne, T., & Resch, B. (2020). From urban stress to neurourbanism: how should we research city well-being? *Annals of the American Association of Geographers*, *110*(6), 1936–1951.

Qian, S., & Chen, D. (1999). Joint time-frequency analysis. *IEEE Signal Processing Magazine*, *16*(2), 52–67.

Rajmohan, V., & Mohandas, E. (2007). The limbic system. *Indian Journal of Psychiatry*, *49*(2), 132–139.

Rao, N. S., & Moharir, P. S. (1998). A signal-dependent evolution kernel for Cohen class time–frequency distributions. *Digital Signal Processing*, *8*(3), 158–165.

Ritter, P., & Villringer, A. (2006). simultaneous EEG–fMRI. *Neuroscience & Biobehavioral Reviews*, *30*(6), 823–838.

Rodrigues, J., Weiß, M., Hewig, J., & Allen, J. J. B. (2021). EPOS: EEG processing open-source scripts. *Frontiers in Neuroscience*, *15*, 660449.

Rosenkranz, K., & Lemieux, L. (2010). Present and future of simultaneous EEG-fMRI. *Magnetic Resonance Materials in Physics, Biology and Medicine*, *23*, 309–316.

Salehinejad, M. A., Ghanavati, E., Rashid, M. H. A., & Nitsche, M. A. (2021). Hot and cold executive functions in the brain: A prefrontal-cingular network. *Brain and Neuroscience Advances*, *5*, 23982128211007770.

Salgado, S., & Kaplitt, M. G. (2015). The nucleus accumbens: a comprehensive review. *Stereotactic and Functional Neurosurgery*, *93*(2), 75–93.

Seery, G. E. (2002). Surgical anatomy of the scalp. *Dermatologic Surgery*, *28*(7), 581–587.

Serai, S. D., Ho, M.-L., Artunduaga, M., Chan, S. S., & Chavhan, G. B. (2021). Components of a magnetic resonance imaging system and their relationship to safety and image quality. *Pediatric Radiology*, *51*, 716–723.

Shad, E. H. T., Molinas, M., & Ytterdal, T. (2020). Impedance and noise of passive and active dry EEG electrodes: a review. *IEEE Sensors Journal*, *20*(24), 14565–14577.

Shekhar, S., & Aryal, J. (2019). Role of geospatial technology in understanding urban green space of Kalaburagi city for sustainable planning. *Urban Forestry & Urban Greening*, *46*, 126450.

Singh, U. K., Prajapati, R., & Kumar, T. (2018). Geological stratigraphy and spatial distribution of microfractures over the Costa Rica convergent margin, Central America–a wavelet-fractal analysis. *Geoscientific Instrumentation, Methods and Data Systems*, *7*(2), 179–187.

Sinha, S., Routh, P. S., Anno, P. D., & Castagna, J. P. (2005). Spectral decomposition of seismic data with continuous-wavelet transform. *Geophysics*, *70*(6), P19–P25.

Spearman's correlation. (n.d.).

Strotzer, M. (2009). One century of brain mapping using Brodmann areas. *Clinical Neuroradiology*, *19*(3), 179.

Suárez-Revelo, J. X., Ochoa-Gómez, J. F., & Tobón-Quintero, C. A. (2018). Validation of EEG pre-processing pipeline by test-retest reliability. *Applied Computer Sciences in Engineering: 5th Workshop on Engineering Applications, WEA 2018, Medellín, Colombia, October 17-19, 2018, Proceedings, Part II 5*, 290–299.

T2 vs T2 relaxation time - Questions and Answers in MRI*. (2023). https://mriquestions.com/t2-vs-t2.html

Teplan, M. (2002). Fundamentals of EEG measurement. *Measurement Science Review*, *2*(2), 1–11.

The 10-20 System for EEG - Electrophysiological Research Blog, News & Events - TMSi. (2022). https://info.tmsi.com/blog/the-10-20-system-for-eeg

The t-Test | Introduction to Statistics | JMP. (2023). https://www.jmp.com/en_ch/statistics-knowledge-portal/t-test.html

The Wet-EEG Cap: Semi-Dry, Saline & Gel EEG caps | Bitbrain. (2018). https://www.bitbrain.com/blog/wet-eeg-cap

Van Hoornweder, S., Mora, D. A. B., Depestele, S., Frieske, J., van Dun, K., Cuypers, K., Verstraelen, S., & Meesen, R. (2022). Age and interlimb coordination complexity modulate oscillatory spectral dynamics and large-scale functional connectivity. *Neuroscience*, *496*, 1–15.

Variação na tensão da rede, porque ocorre? - Mundo da Elétrica. (2023). https://www.mundodaeletrica.com.br/variacao-na-tensao-da-rede-porque-ocorrer/

Verano, J. W. (2016). Differential diagnosis: trepanation. *International Journal of Paleopathology*, *14*, 1–9.

Wacker, J., Dillon, D. G., & Pizzagalli, D. A. (2009). The role of the nucleus accumbens and rostral anterior cingulate cortex in anhedonia: integration of resting EEG, fMRI, and volumetric techniques. *Neuroimage*, *46*(1), 327–337.

Westbrook, C., & Talbot, J. (2018). *MRI in Practice*. John Wiley & Sons.

What is a neuron? - Queensland Brain Institute - University of Queensland. (n.d.). Retrieved September 23, 2023, from https://qbi.uq.edu.au/brain/brain-anatomy/what-neuron

Wu, M.-T. (2019). Wavelet transform based on Meyer algorithm for image edge and blocking artifact reduction. *Information Sciences*, *474*, 125–135.

Xu, J., Mitra, S., Van Hoof, C., Yazicioglu, R. F., & Makinwa, K. A. A. (2017). Active electrodes for wearable EEG acquisition: Review and electronics design methodology. *IEEE Reviews in Biomedical Engineering*, *10*, 187–198.

Zhu, X., Gao, M., Zhang, R., & Zhang, B. (2021). Quantifying emotional differences in urban green spaces extracted from photos on social networking sites: A study of 34 parks in three cities in northern China. *Urban Forestry & Urban Greening*, *62*, 127133.

10. Annexes

10.1. Experiment Devices

- **EEG Amplifier**: Captures and amplifies the participant's EEG and ECG signals. Other features: it acts as a Faraday cage and reduces noise produced by the MRI environment.

***Figure 10.1**: EEG amplifier.*

- **Voltage Regulator**: Keeps the mains voltage of all connected devices at a safe level and avoid potential voltage spikes from the power supply. If there are large voltage fluctuations, the device can be overloaded and eventually damaged (*Variação Na Tensão Da Rede, Porque Ocorre? - Mundo Da Elétrica*, 2023).

***Figure 10.2**: Voltage regulator.*

- **Power Supply**: Provides power to the equipment, namely the EEG amplifier.

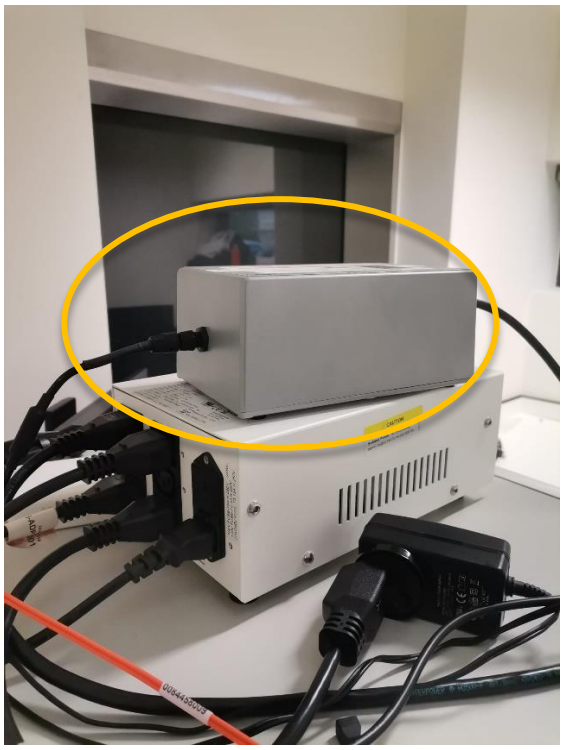

***Figure 10.3**: Power supply.*

- **Router**: Enables TCP/IP communication between the acquisition computer and the EEG amplifier.

***Figure 10.4**: Router.*

- **GES Clock Sync I/0**: Synchronize the clocks of EEG and MRI scanner. It receives and converts the triggers signal arriving from the MRI (converts from analogue to digital signal). Basically, clock sync I/O is a crucial procedure in a variety of systems, ensuring that hardware and software components can coexist peacefully and yield excellent outcomes.

Figure 10.5*: GES clock sync I/O.*

- **Joysticks**: They are used for the participant to score the pictures. The buttons are assigned: low left = 1, low right = 2, upper left = 3, and upper right = 4.

Figure 10.6: *Joysticks. Retrieved from* (FMRI Response Grips | Social, Life, and Engineering Sciences Imaging Center, 2023).

- **Fibre Optic Cables**: Fibre-optic cables have a higher capacity for transmitting information, in addition to having a higher transmission speed than ordinary metal cables, and do not suffer interference from other electromagnetic waves (*Fibra Óptica - InfoEscola,* n.d.). They are used to

conduct the data from the EEG amplifier to the acquisition computer, and to conduct the trigger signal between the GES Clock Sync I/O and the EEG amplifier.

***Figure 10.7**: Fibre optic cables.*

- **Joysticks Interface Box**: Receives the signals from the joysticks. It has 4 lights that light up according to the score the subject gives to each image. The scoring scale is, from left to right: 2, 1, 4 and 3.

***Figure 10.8**: Joysticks interface box.*

- **Stimbox**: Contains the MRI pre-sets, that is, the definition of volumes, slices, etc. For this experiment, it is used 320 volumes and 35 slices. The triggers that come from the MRI and the joysticks signals come to this box to be sent to the stimulus computer. The communication between MRI, joysticks, and the stimbox follows a serial protocol.

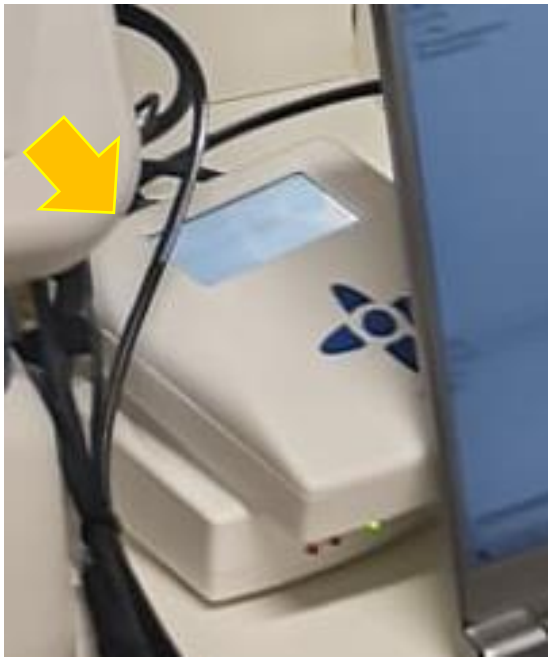

***Figure 10.9**: Stimbox.*

- **EEG Acquisition Computer**: Where the EEG data is stored. Therefore, it features the software that allows recording the data (*Net Station Acquisition* (*Net Station Acquisition for Routine EEG Data Collection: Video Tutorial*, 2021)), as well as the one that allows scanning the EEG electrodes (*GeoScan* (*GeoScan Handheld Sensor Digitization*, 2021)).

***Figure 10.10**: EEG acquisition computer.*

- **Stimulus Computer**: The full experiment protocol developed in *Psychtoolbox* (Pelli & Vision, 1997) toolbox in *MATLAB* (Matlab, 2012) is executed here, and stimuli are shown via HDMI to a screen inside the MRI room.

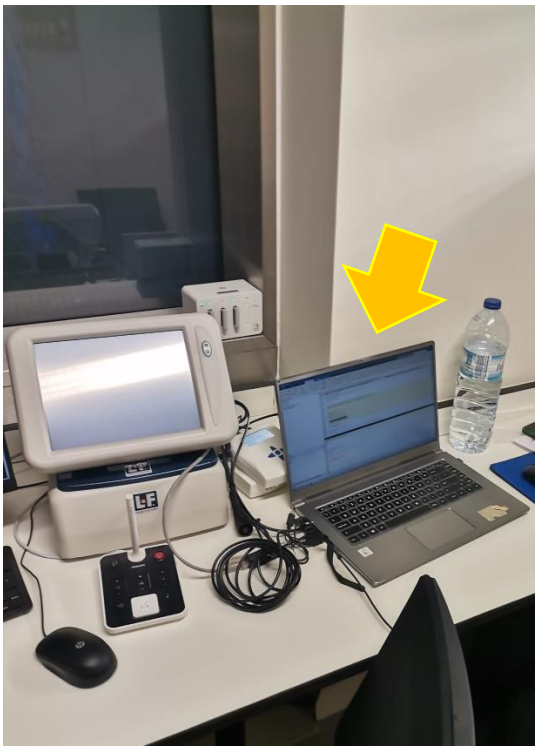

***Figure 10.11**: Stimulus computer.*